1984

Lifetime measurements of some S and D states of K I.

D'Arcy J. Hart
University of Windsor

CANADIAN THESES

THÈSES CANADIENNES

NOTICE

The quality of this microfiche is heavily dependent upon the quality of the original thesis submitted for microfilming. Every effort has been made to ensure the highest quality of reproduction possible.

If pages are missing, contact the university which granted the degree.

Some pages may have indistinct print especially if the original pages were typed with a poor typewriter ribbon or if the university sent us an inferior photocopy.

Previously copyrighted materials (journal articles, published tests, etc.) are not filmed.

Reproduction in full or in part of this film is governed by the Canadian Copyright Act, R.S.C. 1970, c. C-30. Please read the authorization forms which accompany this thesis.

AVIS

La qualité de cette microfiche dépend grandement de la qualité de la thèse soumise au microfilmage. Nous avons tout fait pour assurer une qualité supérieure de reproduction.

S'il manque des pages, veuillez communiquer avec l'université qui a conféré le grade.

La qualité d'impression de certaines pages peut laisser à désirer, surtout si les pages originales ont été dactylographiées à l'aide d'un ruban usé ou si l'université nous a fait parvenir une photocopie de qualité inférieure.

Les documents qui font déjà l'objet d'un droit d'auteur (articles de revue, examens publiés, etc.) ne sont pas microfilmés.

La reproduction, même partielle, de ce microfilm est soumise à la Loi canadienne sur le droit d'auteur, SRC 1970, c. C-30. Veuillez prendre connaissance des formules d'autorisation qui accompagnent cette thèse.

THIS DISSERTATION
HAS BEEN MICROFILMED
EXACTLY AS RECEIVED

LA THÈSE A ÉTÉ
MICROFILMÉE TELLE QUE
NOUS L'AVONS REÇUE

NL 339 (r. 86/01)

Canada

LIFETIME MEASUREMENTS OF SOME S AND D STATES OF K I

by

D'ARCY J. HART

A Thesis
submitted to the
Faculty of Graduate Studies and Research
through the Department of Physics
in Partial Fulfillment
of the requirements for the Degree
of Master of Science at
the University of Windsor

Windsor, Ontario

ABSTRACT

The direct radiative lifetimes of the $6S_{1/2}$ -$12S_{1/2}$, $5D_{3/2}$ -$6D_{3/2}$, $5D_{5/2}$ -$6D_{5/2}$ and 7D-10D levels of potassium have been measured using the time-resolved fluorescence technique after two-photon excitation by a tunable dye laser. In the case of the $3D_{3/2}$ and $3D_{5/2}$ levels, single photon quadrupole excitation was used while the cascade transition from the $4P_{3/2}$ had to be viewed instead of the direct transition to the $4P_{1/2}$ or $4P_{3/2}$ level as in the other levels. An attempt was made to measure the lifetimes of the $4D_{3/2}$ and $4D_{5/2}$ levels by both of the above methods but there was no fluorescence yield distinguishable from noise in either case.

Both Zeeman and hyperfine quantum beats were effectively removed from the fluorescence signal by counteracting the earth's magnetic field and by use of a polarizer set at the 'magic angle' respectively. The data was analysed using a non-linear (exponential-fitting), least-squares fit computer program to yield both the lifetime and statistical standard deviation for one or two components of the decay curve.

The experimental results are compared to previous measurements (if any) and to theoretical calculations based on the Coulomb approximation and corrected for spin-orbit interaction and blackbody radiation induced depopulation effects. The results are also compared to theoretical results based on hydrogenic wavefunctions as a function of effective principal quantum number (n*).

ACKNOWLEDGEMENTS

The author would like to thank Dr.J.B.Atkinson for acting as supervisor for this project and for suggestions in the solution of experimental, theoretical and computer problems. Also, I would like to thank Dr.R.Niefer for aid in the set-up and understanding of much of the apparatus, especially the lasers.

Finally, acknowledgements go to A.Ditchburn (glasswork), B.Masse (electronics), the Physics Machine Shop and D.Giers for the building of or obtaining of equipment and information. Also, thanks to A.Buzzeo for aid in the drawing of the figures appearing in this thesis.

TABLE OF CONTENTS

LIST OF TABLES

LIST OF FIGURES

INTRODUCTION

Up until the present there have been few investigations into the effects of the spin-orbit interaction on absolute line strengths, either experimental or theoretical. The majority of such investigations deal with the alkali atoms because of their similarity in electron configuration to the hydrogen atom and the ease with which they can be worked experimentally.

Tables for the theoretical calculation of transition probabilities in the alkalis have been computed by various authors including Bates and Damgaard[1](1949), Warner[2](1967) and Edmonds et al.[3](1979). However, only Warner allowed for the spin-orbit interaction in his calculations. None of these tables is extensive enough to allow for calculation of lifetimes for higher-lying levels in the potassium atom. This would necessitate further calculations if comparison with experimental results is desired.

The method normally used for calculation of transition probabilities (or Einstein A coefficients) involves inward integration of the Schrodinger equation to obtain the wavefunctions for the two levels concerned in the transition. The degree of accuracy of the result will depend upon the Hamiltonian used for each level and the form of the potential used for the single valence electron. A Coulomb approximation to the potential function is typically used although more complicated approximations are required if one desires greater accuracy for the wavefunctions at small radii. Contributions to the wavefunction integral for small radii are usually negligible, necessitating the choosing of a cut-off criterion for the integral. Otherwise, the integral would blow up near the origin due to the Coulomb approximation. There are no hard and fast rules for the cut-off choice for which reason this method has gained some reputation for inaccuracy, especially in the cases where $n^* < \ell+1$ for the levels concerned.

Nevertheless, good agreement with experimental results can be achieved if the natural radiative lifetimes derived from this method are modified by theoretical calculations of blackbody radiation induced stimulated emission and absorption effects and collisional depopulation effects.

Initially, experimentation could only employ one-photon excitation (using a variety of methods) to populate an excited level. This was due to equipment limitations for the photon source, restricting the measurement of direct lifetimes in the alkali atoms to the P levels. Measurements of S and D state lifetimes could be made but only by the less accurate cascade method. That is, the S and D levels had to be populated from a higher-lying P level instead of directly from the ground state. Only recently have high-powered, tunable dye lasers become available making possible either direct excitation of S and D levels using a virtual intermediate level and two photons of the same wavelength or stepwise excitation using a real intermediate level and two photons of different wavelengths. The same high power also allows for single-photon, quadrupole excitation ($\Delta\ell=0,\pm2$).

Previous measurements of the lifetimes of levels in alkali atoms which differentiate between the two fine-structure levels in the D configurations include Teppner and Zimmermann[4] (K-$3D_{3/2}$ and $3D_{5/2}$, Rb-$4D_{3/2}$ and $4D_{5/2}$) and Neil[5] (Cs-$8D_{3/2}$ to $15D_{3/2}$ and $8D_{5/2}$ to $15D_{5/2}$). Other measurements separating fine-structure levels deal mainly with the principal series of the alkalis (see Ref. 5 for further references to Rb and Cs lifetime measurements).

In the case of potassium, the only comprehensive measurement of direct lifetimes of S and D states was performed by Gallagher and Cooke[29] for the 7S-11S and 5D-9D levels. Using stepwise excitation ($4P_{3/2}$ intermediate level) they were able to separately excite the $nD_{5/2}$ or $nS_{1/2}$ level in each case. They assumed that the $nD_{3/2}$ and $nD_{5/2}$ levels would have

the same lifetimes. The fluorescence from the $nD_{5/2}$-$4P_{3/2}$ or $nS_{1/2}$-$4P_{3/2}$ transition was observed.

This method presents two difficulties. Since the transition being viewed has the same wavelength as the photons from the second laser being used, laser scatter might tend to overload the photomultiplier tube employed in the spectrometer. In addition, there is some possibility of radiation trapping. Photons resulting from atoms decaying from the upper S or D states to the $4P_{3/2}$ level might encounter atoms already in the $4P_{3/2}$ excited state and be absorbed, since they have exactly the right wavelength. This would effectively increase the observed lifetime. Though the probability of this occuring is small (and could be checked for by measuring lifetimes at various vapour pressures) it would indicate that two-photon excitation using a virtual intermediate level would be a superior method in this respect. The latter would also be the simpler method, requiring only one laser sytem. One disadvantage to using the virtual intermediate level is the reduction in resolution of fine-structure levels by a factor of two. For example stepwise excitation would only require a bandwidth of 0.04 cm^{-1} for the second laser in order to resolve the nD levels up to n=9 in potassium while the other method would require 0.02 cm^{-1} bandwidth for the single laser.

Other work on the lifetimes of levels in potassium which have some bearing on this investigation include the following:

1.) $4P_{1/2}$ and $4P_{3/2}$ - Copley and Krause[6]
2.) $4P_{1/2}$ and $4P_{3/2}$ - Link[7]
3.) $4P_{3/2}$ and $5P_{3/2}$ - Schmieder and Lurio[8]
4.) $5P_{3/2}$ and $6P_{3/2}$ - Svanberg[9]
5.) $6S_{1/2}$ - Bulos et al.[10]

In this investigation a study will be made of the lifetimes of the $3D_{3/2}$ to $6D_{3/2}$ and $3D_{5/2}$ to $6D_{5/2}$ states with

the purpose of determining the difference between lifetimes of the fine-structure levels of the same D configuration, if any. Additional data will be given on the lifetimes of the $6S_{1/2}$ to $12S_{1/2}$ states and the 7D to 10D states in an attempt to match the experimental lifetimes with the theoretical lifetimes calculated using the method of Warner and corrected for blackbody radiation induced depopulation effects. Collisional depopulation effects will hopefully be eliminated in the experiment. All other possible influences on the decay curve will be minimized. These include quantum beat modulations and radiation trapping effects.

THEORY

In this chapter the time dependence of the fluorescence intensity will be examined including the rate at which an excited level radiatively decays by spontaneous emission and a calculation of this rate for various levels of potassium. The effective reduction of this natural radiative lifetime by blackbody radiation and collisional depopulation effects will also be examined. Finally, the effect of hyperfine splitting in the various fine structure levels on the time dependence of the fluorescence signal will be calculated.

A. Time Evolution of Fluorescence Intensity

When there is a population of atoms in an excited state, the number of atoms in that excited state will decrease by the process of spontaneous emission. If there is no stimulated emission or absorption (that is, no external radiation present) and no collisional depopulation effects, the probability that an excited atom in the state i decays directly to a single final state f is given by the Einstein coefficient A_{if}. In order to find the total probability for transition out of an excited state by spontaneous emission alone, one must sum the A_{if} values over all possible final states such that:

$$A_i = \sum_f [A_{if}] \tag{1}$$

The possible final states are chosen by the selection rules $\Delta\ell=\pm1, \Delta J=0,\pm1 (J=0 \not\rightarrow J=0)$ for the orbital angular and total angular momentum respectively. Each final state must lie below the initial state in energy.

For spontaneous emission alone, the time evolution of the excited state population can thus be described by:

$$dN_i/dt = -A_i N_i \tag{2}$$

which yields:

$$N_i(t) = N_i(0)e^{-A_i t} \tag{3}$$

where $N_i(0)$ is the initial excited state population.

The lifetime (τ) for this level is defined as:

$$(3) \qquad \tau = 1/A_i = \left(\sum_f [A_{if}]\right)^{-1}$$

The total fluorescence produced is divided amongst the possible transitions to the various final states. If only a single transition is actually observed the detected fluorescence is proportional to $N_i A_{if}$ where A_{if} corresponds to the detected transition. The observed fluorescence will still decay in intensity with a lifetime equal to $1/A_i$ however, since the excited state population is still decaying at this rate.

Due to equipment limitations it is not always possible to observe the direct transition out of an excited level. An example is the $3D_{3/2}$ to $4P_{3/2}$ transition in potassium. Instead a cascade transition must be observed ($4P_{3/2}$ to $4S_{1/2}$ in the example given above). Since the direct transition is no longer being observed the rate equations become more complicated.

In the case of the decay of the $3D_{3/2}$ and $3D_{5/2}$ levels of potassium the following rate equations must be solved:

$$(4) \qquad dN_{3D}/dt = -A_{3D}N_{3D}$$

$$(5) \qquad dN_{4P}/dt = -A_{4P}N_{4P} + A_{DP}N_{3D}$$

where A_{4P} = transition probability of $4P_{3/2}$ to $4S_{1/2}$

A_{DP} = transition probability of $3D_{3/2}$ to $4P_{3/2}$ (or $3D_{5/2}$ to $4P_{3/2}$)

A_{3D} = total transition probability for $3D_{3/2}$ level (or $3D_{5/2}$ level)

This yields the solution:

$$(6) \qquad N_{4P} = \frac{A_{DP}N_{3D}(0)}{A_{4P}-A_{3D}} \left[e^{-A_{3D}t} - e^{-A_{4P}t}\right]$$

assuming that the initial population of the $4P_{3/2}$ state is 0. The $4P_{1/2}$ level can also be used instead of the $4P_{3/2}$ level

for viewing the cascade from the $3D_{3/2}$ level.

Using equation (6) one should expect to see for this cascade transition an initial fluorescence signal of zero which then builds up to a maximum and decays exponentially to zero again with time.

B. Calculation of Transition Probabilities

As stated previously, the probability per unit time of an excited state decaying to a certain final state is given by the Einstein A coefficient A_{if} which can be determined theoretically using the equation:

$$(7) \qquad A_{if} = (64\pi^4 \nu_{if}^3 / 3hc^3) |\langle i|e\vec{r}|f\rangle|^2$$

where $|i\rangle$ and $|f\rangle$ denote the initial and final wavefunctions describing these states and $e\vec{r}$ is the electric dipole operator. The techniques of calculating the dipole matrix elements will now be discussed and the results compared to experimental values.

Bates and Damgaard[1] demonstrated that almost the entire contribution to the integral in equation (7) comes from the region in which the valence electron experiences a Coulomb attraction providing the atom has only one valence electron (i.e.,the alkalis). Various authors have attempted to modify this approach to achieve more accurate results (better agreement with experimental results) but at the cost of the simplicity of the Coulomb approach which will now be applied.

The problem is first reduced to calculating the absolute line strength S such that:

$$(8) \qquad A_{if} = (64\pi^4/3h)(\nu^3/g_2)S$$

where ν = frequency of the transition i→f in Rydbergs

g_2 = statistical weight of the upper level.

For transitions in atoms which can be described by L-S

coupling, O.S.Heavens[36] has shown that:

$$(9) \qquad A_{if} = (64\pi^4\nu^3/3h)\left(\frac{S}{2J_i+1}\right)$$
$$= (2.677\times10^9)k\nu^3\sigma^2 \text{ in sec.}^{-1}$$

where ν is expressed in Rydbergs

k is the angular portion of the integral S

σ^2 is the radial portion of the integral S containing the factor $[\int_o^\infty R_i(r)R_f(r)rdr]^2$

The wavefunctions $R_{n\ell}$ can be found from the solution of the Schrodinger equation:

$$(10) \qquad \frac{d^2R_{n\ell}(r)}{dr^2} - [V(r) + \frac{\ell(\ell+1)}{r^2} - E + H(r)]R_{n\ell} = 0$$

where $V(r) = 2(N-Z)/r$ in the Coulomb approximation

$H(r)$ includes all other interactions

E is the energy of the n,ℓ level

Neglecting $H(r)$ the standard form of solution for $R_{n\ell}$ is in terms of hypergeometric functions:

$$(11) \qquad R_{n\ell}(r) = (-1)^{n+\ell+1}(Z-N)^{1/2}K(n^*,\ell)\left(\frac{2\rho}{n^*}\right)^{n^*}$$
$$\times\, e^{-\rho/n^*}\sum_{t=0}^{t_o}[a_t(n^*,\ell)\rho^{-t}]$$

where $\rho = (Z-N)/r$ ($N = Z$ - degree of ionization of atom + 1)

Energy parameter $\epsilon = \dfrac{E(\text{ionization}) - E_{n\ell}}{R_K} = 1/(n^*)^2$

which defines n^*, the principal effective quantum number and the quantum defect parameter (μ) as a function of ϵ such that $\mu(\epsilon) = n - n^*$ and $R_K = 109735.78\ \text{cm}^{-1}$

$K(n^*,\ell) = [\xi(n^*)n^{*2}\Gamma(n^*+\ell+1)\Gamma(n^*-\ell)]^{-1/2}$

$a_o = 1$, $a_t = a_{t-1}(n^*/2t)[\ell(\ell+1)-(n^*-t)(n^*-t+1)]$

$\xi(n^*) = 1 + [(2/n^{*3})(\partial\mu(\epsilon)/\partial\epsilon)]$

For potassium $\mu(\epsilon)$ was calculated for the various levels using the energy levels given by Corliss and Sugar[13]. Then μ was fitted to:

$$(12) \qquad \mu(\epsilon) = a_o + b_1 \epsilon + b_2 \epsilon^2 + b_3 \epsilon^3$$

using a least squares fit. The results are shown in Table I.

In terms of computation time it is more efficient to first calculate the radial wavefunctions by inward integration of the Schrodinger equation and then evaluate the integral S. It should be noted in equation (11) that the summation is cut off at some value t_o instead of continuing on to lower values of r (or higher values of ρ). If one uses the Coulomb approximation the wavefunction will tend to blow up as $r \to 0$ ($\rho \to \infty$). Since the region near the origin usually contributes very little to the S integral because of the r term, this region can be ignored in most cases. Thus t_o defines the region to be ignored. The best cutoff criterion (choice of t_o) appears to come from the behaviour of the summation in equation (11). As the terms are added, the sum appears to oscillate up and down at first. Finally it will reach some local minimum before blowing up at infinity. This local minimum defines the best cutoff criterion and gives the value for t_o from the number of terms required to reach this minimum.

Several authors have performed these calculations by a variety of methods. A comparison of their results for some levels of potassium can be seen in Table II.

Bates and Damgaard[1] gave tabulations of $F(n^*, \ell)$ and $I(n^*_{\ell-1}, n^*_\ell, \ell)$ where:

$$F = (3n^*_\ell/2)\left[\frac{n^{*2}_\ell - \ell^2}{4\ell^2 - 1}\right]^{1/2}$$

$$I = \{2/(3n^*_\ell[n^{*2}_\ell - \ell^2]^{1/2})\}\left[\int_o^\infty R_i R_f r dr\right]$$

σ = FI for neutral potassium

In addition, I was calculated using a doubly asymptotic series instead of calculating individual wavefunctions.

TABLE I

Least Squares Fit of $\mu(\epsilon)=a_o+b_1\epsilon+b_2\epsilon^2+b_3\epsilon^3$ for the Energy Levels of Potassium I (Corliss and Sugar)

L_J	a_o	b_1	b_2	b_3
$S_{1/2}$	2.1802	0.1359	0.0793	-0.0621
$P_{1/2}$	1.7131	0.2721	-0.3002	1.5218
$P_{3/2}$	1.7100	0.2714	-0.2774	1.4559
$D_{3/2}$	0.2771	-1.0339	-0.7478	3.8820
$D_{5/2}$	0.2774	-1.0396	-0.6110	3.1379
$F_{5/2,7/2}$	0.0115	-0.2659	6.8309	-60.2066

For $E_{n\ell}/hc = R_K/(n-\mu)^2$ this gives the following fit to Corliss and Sugar's energy levels for the potassium I $nS_{1/2}$ states (in cm^{-1}):

nL_J	C&S	Least Squares Fit
$5S_{1/2}$	21026.551	21026.55
$6S_{1/2}$	27450.692	27450.70
$7S_{1/2}$	30274.28	30274.28
$8S_{1/2}$	31765.37	31765.37
$9S_{1/2}$	32648.35	32648.34
$10S_{1/2}$	33214.215	33214.21
$11S_{1/2}$	33598.54	33598.54
$12S_{1/2}$	33871.46	33871.46

N.B. $R_K = \dfrac{R_\infty M_K}{m_o+M_K}$

where $R_\infty = 109737.31\ cm^{-1}$

M_K is the mass of the potassium nucleus

m_o is the mass of the electron.

TABLE II

Comparison of A Coefficients for Transitions in Potassium I as Calculated by Other Authors

Levels		A Values (1/sec)		
Initial	Final	Bates & Damgaard[1]	Warner[2]	Edmonds et al.[3]
$5S_{1/2}$	$4P_{1/2}$	7.154(6)	7.096(6)	7.303(6)
$5S_{1/2}$	$4P_{3/2}$	1.421(7)	1.433(7)	1.451(7)
$6S_{1/2}$	$4P_{1/2}$	2.216(6)	2.205(6)	2.327(6)
$6S_{1/2}$	$4P_{3/2}$	4.377(6)	4.369(6)	4.611(6)
$6S_{1/2}$	$5P_{1/2}$	1.577(6)	1.568(6)	1.590(6)
$6S_{1/2}$	$5P_{3/2}$	3.128(6)	3.158(6)	3.155(6)
$3D_{3/2}$	$4P_{1/2}$	2.112(7)	2.183(7)	1.577(7)
$3D_{3/2}$	$4P_{3/2}$	4.162(6)	4.283(6)	3.117(6)
$3D_{5/2}$	$4P_{3/2}$	2.495(7)	2.323(7)	1.868(7)
$4D_{3/2}$	$4P_{1/2}$	3.450(3)	9.214(4)	3.568(5)
$4D_{3/2}$	$4P_{3/2}$	1.70(2)	1.165(4)	6.476(4)
$4D_{3/2}$	$5P_{1/2}$	2.964(6)	2.959(6)	2.837(6)
$4D_{3/2}$	$5P_{3/2}$	5.840(5)	5.860(5)	5.591(5)
$4D_{5/2}$	$4P_{3/2}$	8.00(2)	6.288(4)	3.848(5)
$4D_{5/2}$	$5P_{3/2}$	3.500(6)	3.162(6)	3.351(6)

N.B. $7.154(6) = 7.154 \times 10^{6}$

Due to the spin-orbit interaction the total radial wavefunction $\Phi_i(r)$ for a level $|n_i \ell SLJ\rangle$ is a mixture of pure eigenfunctions of all levels with identical ℓSLJ:[27]

$$(13) \qquad \Phi_i(r) = a_i \varphi_i(r) + \sum_{j \neq i} [b_j \varphi_j(r)]$$

For example for the $5P_{1/2}$ level of potassium $a_i \cong 1$, $\varphi_i(r)$ is the radial wavefunction for the $5P_{1/2}$ level and the summation is over the radial wavefunctions for the $4P_{1/2}$, $6P_{1/2}$, $7P_{1/2}$, et cetera levels. Since b_j is inversely proportional to the energy difference between the i and j levels only the j levels lying close to the i level will have much effect.

Warner has taken into account this interaction in his calculations. He has shown that:

$$(14) \qquad \int_o^\infty \Phi_i(r) \Phi_f(r) r dr = I_{ik} + T_i \sum_{j \neq i} \left(\frac{\delta_{ij} I_{jk}}{E_i - E_j}\right) + T_k \sum_{j' \neq k} \left(\frac{\delta_{kj'} I_{j'i}}{E_k - E_{j'}}\right) + T_i T_k \sum_{j \neq i} \sum_{j' \neq k} \left(\frac{\delta_{ij} \delta_{kj'} I_{jj'}}{(E_i - E_j)(E_k - E_{j'})}\right)$$

where $I_{ik} = \int_o^\infty R_i(r) R_f(r) r dr$

$$\delta_{ij} = \left[\left(\ell_i + \tfrac{1}{2}\right)\left(\ell_j + \tfrac{1}{2}\right)\right]_o \int^\infty \zeta(r) R_i^2 dr \int_o^\infty \zeta(r) R_f^2 dr]^{1/2}$$

$$T_i = \frac{J(J+1) - S(S+1) - L(L+1)}{2L+1} \quad \text{for the } n_i \ell_i j_i \text{ level}$$

$$\zeta(r) = \frac{1}{2r} \frac{dV(r)}{dr}$$

$$V(r) = \frac{2(N-Z)}{r} \quad \text{for } r \geq R_o$$

R_o defines the radius of the Thomas-Fermi-Dirac ion whose potential inside this radius deviates from the Coulomb approximation. However, this portion was ignored since the contribution to the integral within R_o is negligible in most cases.

Warner tabulated gf values such that:

$$gf_{ik} = \frac{2}{3} |E_i - E_k| (2L_i + 1)(2L_k + 1) L_> W^2(L_i L_i L_k L_k; 0\ 1)$$

$$x \left[\int_o^\infty \Phi_i(r)\Phi_k(r)rdr\right]^2$$

where $L_>$ is the greater of L_i, L_k

W is the Racah coefficient

In a departure from the Coulomb approximation, Edmonds et al.[3] used an empirical approach based on the work of Naccache (1972). They tabulated $g_p(s)$ values for $0 \le p \le 3$ such that:

$$\int_o^\infty R_i R_f rdr = \left(\frac{3}{2} n_c^{*2}[1-(\ell_c/n_c^*)^2]^{1/2}\right) \sum_{p=o}^{3} \gamma^p g_p(s)$$

where ℓ_c is the greater of ℓ_i, ℓ_f

$n_c^* = 2/(1/n_i^* + 1/n_f^*)$

$\gamma = \Delta\ell(\ell_c/n_c^*)$

$\Delta\ell = \ell_f - \ell_i$

$s = n_i^* - n_f^*$

For a complete analysis of this method one should refer to the literature mentioned.

Since none of these tabulations were extensive enough to calculate up to the 12S or 10D lifetimes of potassium, the method of Warner was adopted to calculate the necessary A coefficients for the purpose of this experiment.

In this case:

$$(15) \qquad I_{ik} = (-1)^{n_i+n_k+\ell_i+\ell_k}(2/n_i^*)^{n_i^*}(2/n_k^*)^{n_k^*}K(n_i^*,\ell_i)$$

$$x\ K(n_k^*,\ell_k) \sum_{p=o}^{p_o} A_p\ \Gamma(n_i^*+n_k^*+2-p)\left(\frac{1}{n_i^*}+\frac{1}{n_k^*}\right)^{p-2-n_i^*-n_k^*}$$

where $A_p = \sum_{t=o}^{p} a_t(n_i^*,\ell_i)a_{p-t}(n_k^*,\ell_k)$

$$(16) \qquad \delta_{ij} = \left[2\left(\ell_i+\frac{1}{2}\right)\left(\ell_j+\frac{1}{2}\right)\right]^{1/2}K(n_i^*,\ell_i)K(n_j^*,\ell_j)(4/n_i^*n_j^*)$$

$$x\left[\sum_{p=o}^{p_o}\Gamma(2n_i^*-2-p)B_{pi}\left(\frac{2}{n_i^*}\right)^p\right]^{1/2}$$

$$x\left[\sum_{q=o}^{q_o}\Gamma(2n_j^*-2-p)B_{qj}\left(\frac{2}{n_j^*}\right)^q\right]^{1/2}$$

where $B_{pi} = \sum_{t=o}^{p} a_t(n_i^*,\ell_i)a_{p-t}(n_i^*)$

$B_{qj} = \sum_{t=o}^{q} a_t(n_j^*,\ell_j)a_{q-t}(n_j^*,\ell_j)$

In each case the criterion for cutoff of a summation was chosen by the procedure given previously on P.11. The results were calculated on a PET-Commodore Series 2001 computer using gamma functions tabulated in Reference 11. The complete results are compiled in Appendix A. The calculated theoretical lifetimes (using equation 3) for the $5S_{1/2}$-$12S_{1/2}$, $3D_{3/2}$-$10D_{3/2}$ and $3D_{5/2}$-$10D_{5/2}$ states are given in Table III.

The above calculations assume no external radiation present at the atom. However, at experimental temperatures (i.e., greater than 0° K) there are blackbody photons present. The resonant components of the blackbody radiation spectrum can induce electric-dipole transitions from the excited level, effectively reducing the observed lifetime from the natural radiative lifetime. This was first demonstrated by Gallagher and Cooke[28]. The latter's theoretical calculations for BBR effects have been shown to be overestimations by Wing and Farley[14]. In a recent paper Wing and Farley calculated more accurately the blackbody correction for alkali atoms at 300° K. Because the transition rates are additive the lifetime equation now becomes:

$$\frac{1}{\tau_0} = \frac{1}{\tau_R} + \frac{1}{\tau_{BB}} \qquad (17)$$

where τ_0 is the observed lifetime

τ_R is the natural radiative lifetime

$$\tau_{BB} = \frac{4e^2}{3\hbar c^3} \sum_f (L_>/(2L_i+1))\left[\int_o^\infty R_i R_f r dr\right]^2 \left(\frac{\omega_{if}^3}{e^{\hbar\omega_{if}/kT}-1}\right)$$

where $L_>$ is the greater of L_i, L_f

ω_{if} is the angular transition frequency

The summation is performed over all possible final states.

The results of Wing and Farley have been used to calculate the effective lifetimes of several levels of potassium, as shown in the second column of Table III, for a temperature of 300° K. It is apparent that the BBR effect

TABLE III

Calculated Lifetimes of Potassium I Levels Using The Coulomb Approximation

Level	Natural Radiative Lifetime (ns)	Reduced Lifetime Due to 300 K BBR (ns)
$5S_{1/2}$	48.3	48.3
$6S_{1/2}$	87.7	87.7
$7S_{1/2}$	158.0	157.4
$8S_{1/2}$	264.5	259.6
$9S_{1/2}$	414.0	397.5
$10S_{1/2}$	614.1	575.0
$11S_{1/2}$	872.2	796.4
$12S_{1/2}$	1191	1062
$3D_{3/2}$	38.5	38.5
$4D_{3/2}$	280.6	280.2
$5D_{3/2}$	578.7	572.4
$6D_{3/2}$	1085	1036
$7D_{3/2}$	1403	1291
$8D_{3/2}$	1742	1553
$9D_{3/2}$	2151	1866
$10D_{3/2}$	2808	2353
$3D_{5/2}$	38.9	38.9
$4D_{5/2}$	282.2	281.8
$5D_{5/2}$	534.0	528.8
$6D_{5/2}$	1097	1047
$7D_{5/2}$	1353	1249
$8D_{5/2}$	1725	1540
$9D_{5/2}$	2215	1914
$10D_{5/2}$	2761	2319

can dramatically reduce the effective lifetimes of higher energy levels in potassium.

C. Calculation of the Fluorescence Intensity Profile

In this section the effect of hyperfine structure splittings on the fluorescence intensity profile will be examined.

It has been found that when a coherent superposition of excited states is populated by the use of a short light pulse, modulation of the fluorescent light decay curve will occur at frequencies corresponding to the excited state energy splittings. These so-called quantum beats will be produced at frequencies corresponding only to the hyperfine structure energy splittings if only one fine structure level is excited and if the atoms are not contained within any appreciable magnetic fields (eliminating Zeeman structure quantum beats).

The intensity profile of the fluorescence signal as seen by a detector can be calculated theoretically. As an observable, the intensity of the signal can be expressed in terms of the excited state density matrix $\sigma_e(t)$ and the operator for detection of fluorescence given by $D(\hat{\varepsilon}_d)$:

$$I(\hat{\varepsilon}_d) \propto \mathrm{Tr}\{\sigma_e(t) D(\hat{\varepsilon}_d)\} \tag{18}$$

where $\hat{\varepsilon}_d$ is the polarization of the light as seen by the detector.

Using irreducible tensor operators, Silverman et al.[18] have shown that the intensity profile after two-photon excitation of the excited level can be expressed by:

$$\begin{aligned} I(\hat{\varepsilon}_d) = K k_o^{(1)}(+\infty) k_o^{(2)}(+\infty) \, \Sigma[(2F_f+1)^{-1/2}(2F_o+1)^{-1/2} \\ \times e^{-i\omega_{F_2F_2'}t} \, e^{-\Gamma t} \\ \times {}^{F_2F_2'}_{k_2q_2}A_{F_fF_f}{}_{o\ o}(\hat{\varepsilon}_d) \; {}^{F_2F_2'}_{k_2q_2}A_{F_1F_1'}{}_{k_1q_1}(\hat{\varepsilon}_2) \; {}^{F_1F_1'}_{k_1q_1}A_{F_oF_o}{}_{o\ o}(\hat{\varepsilon}_1)] \end{aligned} \tag{19}$$

where K is a constant dependent only upon the geometry of the detector;

$k_o^{(1)}(+\infty)$, $k_o^{(2)}(+\infty)$ are factors dependent on the strength of the pumping;

$\vec{F} = \vec{J} + \vec{I}$

$\vec{I}$ is the nuclear spin angular momentum

$\vec{J} = \vec{L} + \vec{S}$ (total angular momentum)

Γ is the radiative decay rate

$\omega_{F_2F_2'}$ is the modulation frequency corresponding to the energy splitting of the hyperfine structure levels F_2 and F_2'

$\hat{\epsilon}_1$ and $\hat{\epsilon}_2$ are the first and second excitation photon polarizations

$\hat{\epsilon}_d$ is the detected light polarization

$A(\hat{\epsilon})$ is a coefficient used in transforming from the density matrix of one level to the density matrix of the next lower level in the sequence $0 \to 1 \to 2 \to f$

The subscripts signify: 0- ground state
1- first excited state (real or virtual)
2-second excited state (real)
f- final state following a direct transition from state 2

The summation in equation 19 is over all possible combinations of F_o, F_1, F_1', F_2, F_2', F_f. For a more detailed derivation of this equation and an explanation of all terms involved the reader should see the two papers of Silverman et al.. The assumptions used in this derivation are the following:

i) Weak pumping $T \ll T_p$

ii) Broadline excitation $\Delta\nu \gg 1/T$

iii) $T \ll \tau_e$

where T = duration of the exciting pulse

T_p = average time between two successive photon absorptions by an atom

τ_e = lifetime of the second excited state

$\Delta\nu$ = bandwidth of laser pulse

In the experiment which follows the above parameters can be estimated as T=10ns, 88ns $\leq \tau_e \leq$ 2300ns and $\Delta\nu$ =1000-1500 MHz. T_p is difficult to estimate but there is the possibility that $T \cong T_p$ which would make the first assumption invalid.

Although Silverman et al. gave an expression for $A(\hat{\epsilon})$ in the second of their papers, only the result and not the derivation was given as applied to fine structure quantum beats. Using graphical methods, the derivation of the expression for $A(\hat{\epsilon})$ as applied to hyperfine structure quantum beats is shown in Appendix B.

Using equation 19 one can calculate the theoretical intensity profile for an excited level in potassium for which the nuclear spin is I=3/2 (for both of the common isotopes). The situation for excitation of an $nD_{3/2}$ level is shown in Figure 1 where a virtual intermediate level has been used in the two-photon excitation process.

The hyperfine splitting of the $D_{3/2}$ and final $P_{1/2}$ levels will produce six quantum beat frequencies, two of which have the same frequency. Assuming that the laser bandwidth is larger than the hyperfine splitting of the $4S_{1/2}$ ground state (462 MHz)[31] the summation for $I(\hat{\epsilon}_d)$ is over:

$F_o = 1,2$

$F_1 = F_1' = 1,2$ for $J_1=1/2$ and $F_1=F_1'=0,1,2,3$ for $J_1=3/2$

The summation is also performed over the following sets of F values corresponding to the second excited state and the final state where the energy splitting between the F_2 and F_2' levels defines the modulation frequency as shown in Figure 1:

(F_2,F_2',F_f) = (0,0,1) or (1,1,1) or (1,1,2) or (2,2,1) or (2,2,2) or (3,3,2) for the unmodulated signal

(F_2,F_2',F_f) = (0,1,1), (1,0,1), for signal modulated at frequency ν_{01}

(F_2,F_2',F_f) = (1,2,1), (1,2,2), (2,1,1), (2,1,2) for signal modulated at frequency ν_{12}

a) The two-photon excitation process followed by the observed direct decay transition for which the intensity profile was calculated.

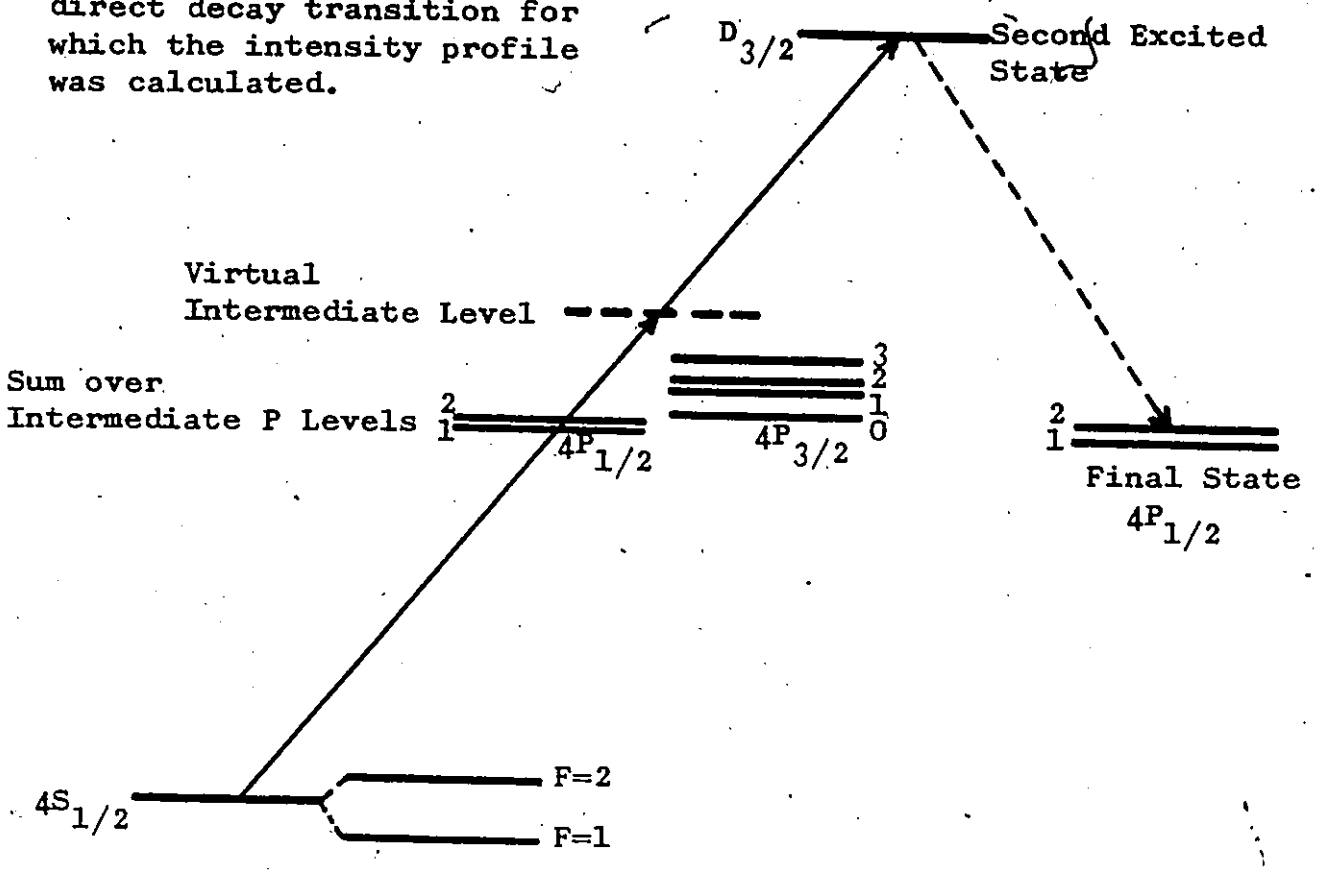

b) The hyperfine structure of the $nD_{3/2}$ levels of potassium. The hyperfine splittings from the unperturbed $D_{3/2}$ level are given by:

$$\Delta\nu = (a_j/2)[F(F+1)-J(J+1)-I(I+1)]$$

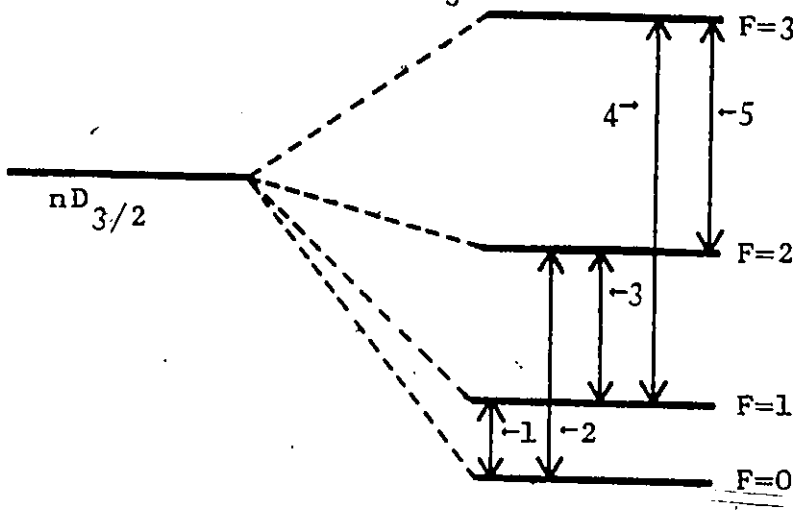

1) $\nu_{01}=a_j$
2) $\nu_{02}=3a_j$
3) $\nu_{12}=2a_j$
4) $\nu_{13}=5a_j$
5) $\nu_{23}=3a_j$

a_j is the magnetic dipole coupling constant.

Figure 1- The absorption and decay processes in potassium used in the calculation of the intensity profile.

$(F_2,F_2',F_f) = (0,2,1), (2,0,1)$, for signal modulated at frequency ν_{02}

$(F_2,F_2',F_f) = (1,3,2), (3,1,2)$ for signal modulated at frequency ν_{13}

$(F_2,F_2',F_f) = (2,3,2), (3,2,2)$ for signal modulated at frequency ν_{23}

In order to simplify the summation, the experimental situation $\varphi_1=\theta_1=0$, $\varphi_2=\theta_2=0$ and $\varphi_d=0$ was chosen. Performing the summation for the $nD_{3/2}$ level gives:(φ,θ are defined in App.B)

$$(20) \qquad I(\theta_d) = K[10.139 + \tfrac{1}{2}(3\cos^2\theta_d-1)(6.351 + 10.952\cos(\omega_{12}t) + 7.187\cos(\omega_{02}t) - 5.389\cos(\omega_{23}t) + 2.245\cos(\omega_{13}t))]$$

where K is a proportionality constant and $\omega_{ij}=2\pi\nu_{ij}$. (See Appendix C for the complete equation.)

It can readily be seen that provided the factor $\frac{1}{2}(3\cos^2\theta_d-1)=0$ (or $\theta_d=54.7^\circ$), there will be no modulation of the signal. Thus, the quantum beats can be eliminated for this situation if the polarization of both exciting photons is linear and parallel to one another and the detected fluorescent light is linearly polarized in a direction 54.7° from the exciting light polarization. This would necessitate the use of a linear analyzer between the fluorescing atoms and the detector.

D. Collisional Perturbations

For the $nD_{3/2,5/2}$ states examined in this experiment, it is possible to get collisional mixing between these two close lying states by collisions of excited state atoms with ground state atoms if the vapour pressure is high enough. This would depopulate the excited state $nD_{3/2}$ into the $nD_{5/2}$ state or vice-versa effectively reducing the observed lifetime. The $nS_{1/2}$ states depopulate predominantly to the $(n-4)F_{5/2,7/2}$

states. Collisional mixing between the $nD_{3/2,5/2}$ and $(n+1)P_{1/2,3/2}$ states or between the $(n-4)G$, $(n-4)H$ and the $nS_{1/2}$ states will be ignored since they become significant only at much higher vapour pressures.

Collisional mixing between dominant partners causes the introduction of an additional exponential component in the fluorescence signal. However, it can be shown that,at the vapour pressures used in this experiment, the additional component should have negligible effect.

If the cross-section for collisional mixing is represented by σ_{ij} then:

$$\gamma_{ij} = \sigma_{ij}\bar{V}\nu \qquad (21)$$

where γ_{ij} is the collisional depopulation rate from level i to level j

$\bar{V}$ is the mean relative velocity of atoms

ν is the vapour density in atoms/meter^3

By solving the population rate equations for levels i and j when collisional effects are included it can be shown that:[23]

$$N_i(t) = \left(\frac{N_o\gamma_{ji}}{\lambda_+-\lambda_-}\right)\left[e^{-\lambda_+t} - e^{-\lambda_-t}\right] \qquad (22)$$

$$N_j(t) = \frac{N_o}{\lambda_--\lambda_+}\left[(\lambda_--\Gamma_j-\gamma_{ji})e^{-\lambda_+t} + (\Gamma_j+\gamma_{ji}-\lambda_+)e^{-\lambda_-t}\right] \qquad (23)$$

where N_o is the initial population of state j

$N_i(0)=0$

Γ_i and Γ_j are the free-atom radiative rates for states i and j respectively

$$\lambda_+ = \frac{1}{2}(\Gamma_i+\Gamma_j+\gamma_{ji}+\gamma_{ij}) + \frac{1}{2}\left[(\Gamma_i-\Gamma_j)^2+2(\Gamma_i-\Gamma_j)(\gamma_{ij}-\gamma_{ji}) + (\gamma_{ij}+\gamma_{ji})^2\right]^{1/2}$$

$$\lambda_- = \frac{1}{2}(\Gamma_i+\Gamma_j+\gamma_{ji}+\gamma_{ij}) - \frac{1}{2}\left[(\Gamma_i-\Gamma_j)^2+2(\Gamma_i-\Gamma_j)(\gamma_{ij}-\gamma_{ji}) + (\gamma_{ij}+\gamma_{ji})^2\right]^{1/2}$$

For the $nS_{1/2}$ and $(n-4)F_{5/2,7/2}$ dominant partners at low vapour pressures these equations reduce to:

$$(24) \qquad N_F(t) = \frac{N_o \gamma_{SF}}{\lambda_- - \lambda_+}[e^{-\lambda_+ t} - e^{-\lambda_- t}]$$

$$(25) \qquad N_s(t) = N_o e^{-\lambda_- t}$$

where $\lambda_+ = \Gamma_{F_{5/2,7/2}} + \gamma_{FS}$

$\lambda_- = \Gamma_{S_{1/2}} + \gamma_{SF}$

Thus, the $nS_{1/2}$ states should decay radiatively with a lifetime given by $[\Gamma_{nS} + \gamma_{SF}]^{-1}$.

Collisional cross-sections for potassium S levels have not as yet been measured experimentally. Hugon et al. have devised an empirical equation for σ_{ij} based upon their measurements of σ_{ij} for rubidium and cesium S and D levels:[26]

$$(26) \qquad \sigma_{ij} = \pi \langle r_e^2 \rangle = \frac{\pi}{2}(n_i^*)^2[5(n_i^*)^2 + 1 - 3\ell_i(\ell_i+1)]a_o^2$$

where n_i^* is the effective principal quantum number of the i^{th} level

a_o is the Bohr radius

For the experimental situation used in this investigation the effect of collisional depopulation would only be significant for levels having a lifetime larger than 1000ns or a collisional cross-section greater than 10^{-16} meter^2. Based upon the above empirical equation (26) there is the possibility that $\sigma > 10^{-16}$ m^2 for the $11S_{1/2}$ and $12S_{1/2}$ levels. Theoretically this would represent possible errors of about 1% and 2% respectively at a vapour pressure of 8×10^{-6} Torr (T=90° C) and using the radiative decay rates listed in Table III. Measuring the lifetimes of these levels at a lower potassium temperature and vapour pressure would assist in reducing this error at the cost of reducing the fluorescence signal also.

For the $nD_{3/2,5/2}$ dominant partners the fact that $\Gamma(D_{3/2})$

is very close to $\Gamma(D_{5/2})$, if not equal to, changes the approximations for λ_+ and λ_- at low vapour pressures. Thus, if $\Gamma(D_{3/2}) \cong \Gamma(D_{5/2})$ then:

$$\lambda_+ = \Gamma(D_{3/2}) + \gamma(D_{5/2} \rightarrow D_{3/2}) + \gamma(D_{3/2} \rightarrow D_{5/2})$$
$$\lambda_- = \Gamma(D_{3/2})$$

If the $nD_{3/2}$ state is initially populated, its population will decay according to:

$$(27) \qquad N_{D_{3/2}}(t) = \frac{N_o}{\gamma_{3/2,5/2}+\gamma_{5/2,3/2}}\left[\gamma_{3/2,5/2}e^{-\lambda_+ t} + \gamma_{5/2,3/2}e^{-\lambda_- t}\right]$$

Only when the vapour pressure is low enough that $\gamma_{3/2,5/2}+\gamma_{5/2,3/2}$ becomes insignificant compared to $\Gamma(D_{3/2})$ will $N_{D_{3/2}}(t)=N_o e^{-\Gamma(D_{3/2})t}$ be true.

Since $\gamma_{3/2,5/2} \cong \left(\frac{g_{5/2}}{g_{3/2}}\right)\gamma_{5/2,3/2}$

where the statistical weights $g_{5/2}$ and $g_{3/2}$ are for the $D_{5/2}$ and $D_{3/2}$ levels and are equal to 6 and 4 respectively, then:

$$\gamma_{3/2,5/2} + \gamma_{5/2,3/2} = \frac{5}{2}\gamma_{3/2,5/2}$$

Using estimates for $\sigma_{3/2,5/2}$ from the empirical equation (26) one finds possible errors of 6% and 7% for the lifetimes of the $9D_{3/2}$ and $10D_{3/2}$ levels at a temperature of 90° C. Lower levels would have insignificant collisional effects at this temperature. A measurement of the $10D_{3/2}$ level lifetime at potassium temperatures ranging from 70° C-120° C would determine if collisional effects are significant if any systematic variation in the lifetime became evident.

METHOD

In order to populate the desired S or D state in potassium several methods are possible. Only the P levels can be populated by single-photon, electric-dipole transitions. Thus, the S and D states could only be populated by cascade transitions from the P levels if this method were used. In addition, because of the energy level structure of potassium and the lower wavelength limit for dye laser operation, only the nP levels for $n \leq 6$ could be populated, severely restricting the number of S and D states which could be reached. Finally, this cascade method would complicate the analysis of the fluorescence signal.

In going from the $4S_{1/2}$ ground state of potassium to a higher lying S or D state there is a change in L of 0 or 2 respectively. These S and D states can only be populated directly by employing either two successive single-photon, electric-dipole transitions ($\Delta L = \pm 1$) or a single-photon, quadrupole transition ($\Delta L = \pm 2$). The former method can use either non-resonant, direct excitation by means of a virtual intermediate level or resonant stepwise excitation using a real intermediate level. For the reasons stated in the Introduction, the non-resonant method was used in this investigation. All of these methods are illustrated in Figure 2.

The cross-section for the non-resonant process is inversely proportional to the energy difference between the virtual intermediate level and the closest lying real level (the 4P levels in this case- see Figure 2). Since the virtual level always lies slightly above the 4P levels one should expect to see a marked decrease in the fluorescence signal as higher lying levels are excited.

Quadrupole transitions, whose cross-sections are typically much smaller than those of electric-dipole transitions, can nevertheless be used to excite the lower D levels of potassium which would be unattainable by two-photon excitation. For the

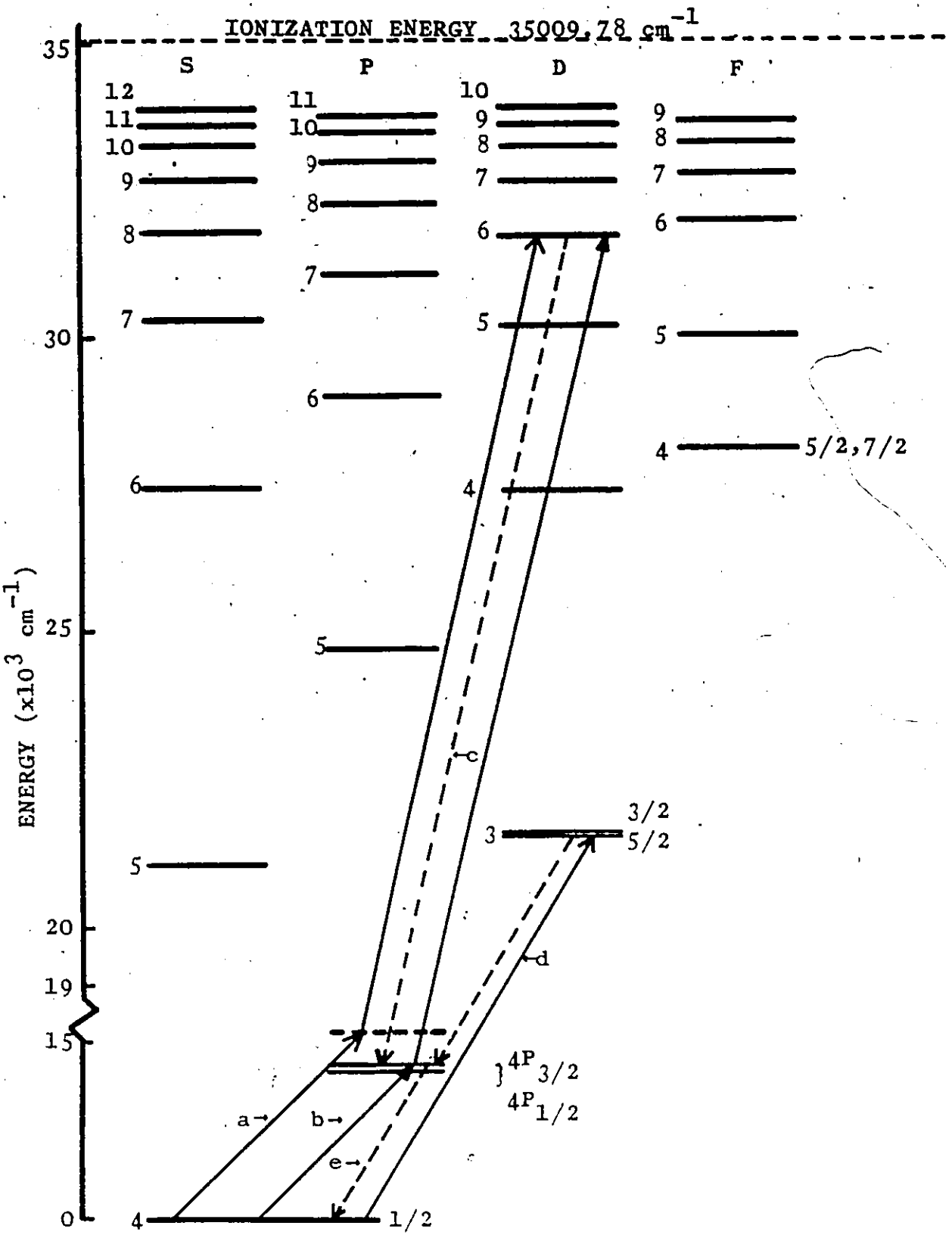

Figure 2- K I Energy Level Diagram
Transitions shown:

a) Non-resonant excitation (virtual intermediate level).
b) Stepwise excitation (real intermediate level).
c) Direct transition out of second excited state.
d) Single-photon, quadrupole excitation.
e) Cascade transition from initially excited 3D level.

3D levels of potassium two-photon excitation would require a laser beam wavelength of 9286Å ($D_{3/2}$) or 9287Å ($D_{5/2}$). Since dyes were unavailable for this wavelength, it was easier to use quadrupole excitation requiring only one photon of wavelength 4643Å ($D_{3/2}$) or 4643.5Å ($D_{5/2}$). The only direct transitions out of the 3D levels are to the 4P levels which emit photons in the infra-red region (about 11700Å). Since these photons could not be detected by the spectrometer being used the cascade transition from the $4P_{1/2}$ or $4P_{3/2}$ level must be viewed with suitable measures taken to avoid radiation trapping.

Instead of using the collision-free and Doppler broadening-free atomic beam method with its inherent technical difficulties it was decided to contain pure potassium in a temperature and pressure controlled fluorescence cell with entrance and exit windows for the laser beam and fluorescence only. The spectrometer for detection of this fluorescence must be capable of delivering amplified electrical pulses corresponding to individual fluorescence photons to a transient digitizer. The digitizer must be able to time resolve the electrical pulses after each laser pulse with a minimum resolution of 1/250 of a lifetime per channel in order that the 1023 channels available will scan at least four lifetimes.

In most cases the direct transition from the excited S or D state to the $4P_{1/2}$ or $4P_{3/2}$ level had the largest branching ratio and was selectively viewed through a monochromator. Then the accumulated data could be analysed for a single decay component with either a non-linear (exponential-fitting) program as applied to the raw data or a linear least-squares fit of a semi-log plot of the data.

For the 3D levels already mentioned the data for the decay curve would have to be analysed for two decay components. With suitable modifications the first computer program mentioned above could also be used for this analysis.

DESCRIPTION OF APPARATUS

Schematic drawings of the apparatus are given in Figures 3 and 4. The potassium S and D levels were populated by two-photon excitation using a Nd:YAG-pumped dye laser. The pumping laser was the Quanta-Ray DCR-1A laser system using a KD*P second harmonic generator crystal to frequency double the 10640Å fundamental output of the laser with approximately 30% conversion efficiency. The second harmonic was separated from the fundamental by means of a Pellin-Broca prism and then directed by a CVI high-power laser mirror (coated for 5320Å) into a three-stage homemade dye laser.

About 5% of the Nd:YAG output was passed through a beam splitter into a 100% reflector which re-directed this beam so as to transversely pump the oscillator stage of the dye laser. The remaining 95% of the YAG output was then divided by means of a 100% reflector, 25% beam splitter and totally reflecting prism to transversely pump the remaining two stages (25% to pre-amplifier and 75% to amplifier). For the purpose of increasing laser effitiency and reducing spontaneous amplification a delay was incorporated between the pumping of the oscillator stage and the pumping of the amplification stages. In other words, the amplifier stages did not commence their pumping until the pulse pumping the oscillator stage had allowed the oscillator to reach threshold.[37] The three transverse pump beams were focussed onto three separate dye cells using cylindrical quartz lenses of 5 cm. diameter.

The dye laser was operated in a Littrow configuration using a Bausch and Lomb 52 mm. square, 600 line per mm. density diffraction grating. With a 54 degree blaze angle, the grating was typically used in fourth or fifth order (52 degrees-71 degrees to the vertical). It was used in conjunction with a 28x quad-prism beam expander[37] so as to cover the full ruled width of the grating with the oscillator output.

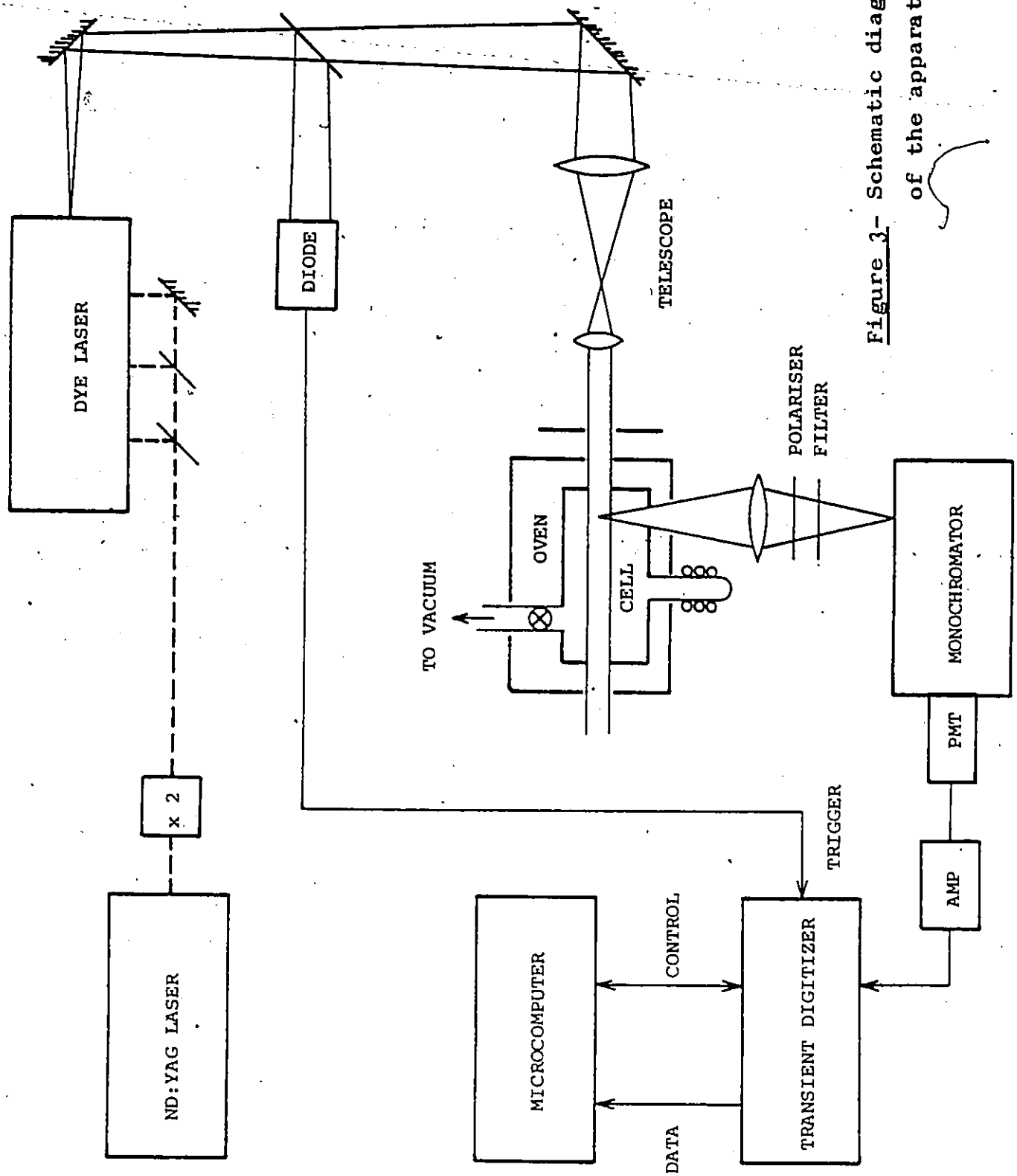

Figure 3- Schematic diagram of the apparatus.

The grating angle was adjusted with a micrometer screw resting against a rotatable arm holding the grating such that the change in wavelength per smallest micrometer division (0.001 inches) was roughly $1.6\cos\theta$ Å in fourth order and $1.3\cos\theta$ Å in fifth order for a grating angle of θ degrees to the vertical.

The Q-switched Nd:YAG laser produced 10ns pulses (FWHM) at a 10Hz rate using only the oscillator stage with a flash-lamp output of 55-60 Joules per pulse. The conversion efficiencies of various laser components in addition to the efficiencies of the dyes used reduced the dye laser output to about 0.5 mJ (Oxazine 725) to 4.0 mJ (Rhodamine 610) per pulse at the entrance to the fluorescence cell, as measured by a Scientech 363 power meter. The efficiencies of the dyes were estimated to range from 4% (Oxa725) to 17% (Rh610).

In order to separately excite the $nD_{3/2}$ and $nD_{5/2}$ levels it was necessary to install a Fabry-Perot etalon in the dye laser oscillator cavity. By monitoring the output with a Quanta-Ray etalon (1 cm^{-1} free spectral range) the laser beam linewidth was found to be 0.2-0.4 cm^{-1} without the F-P etalon installed while it was reduced to 0.04-0.07 cm^{-1} with the etalon. Since two-photon excitation was being employed, this made it possible to satisfactorily separate only the nD levels for $n \leq 6$ (the 7D levels are separated by 0.13 cm^{-1} and the separation decreases as n increases). The orientation of the F-P etalon was adjusted by hand for fine tuning of the wavelength in conjunction with the micrometer screw. The output of the dye laser was collimated and adjusted for spot size using a telescopic lens arrangement between the pre-amplifier and amplifier stages.

Since the 3371Å output of the nitrogen laser is better suited to pumping the dye necessary to reach the 3D levels in single-photon, quadrupole excitation, a two stage dye laser

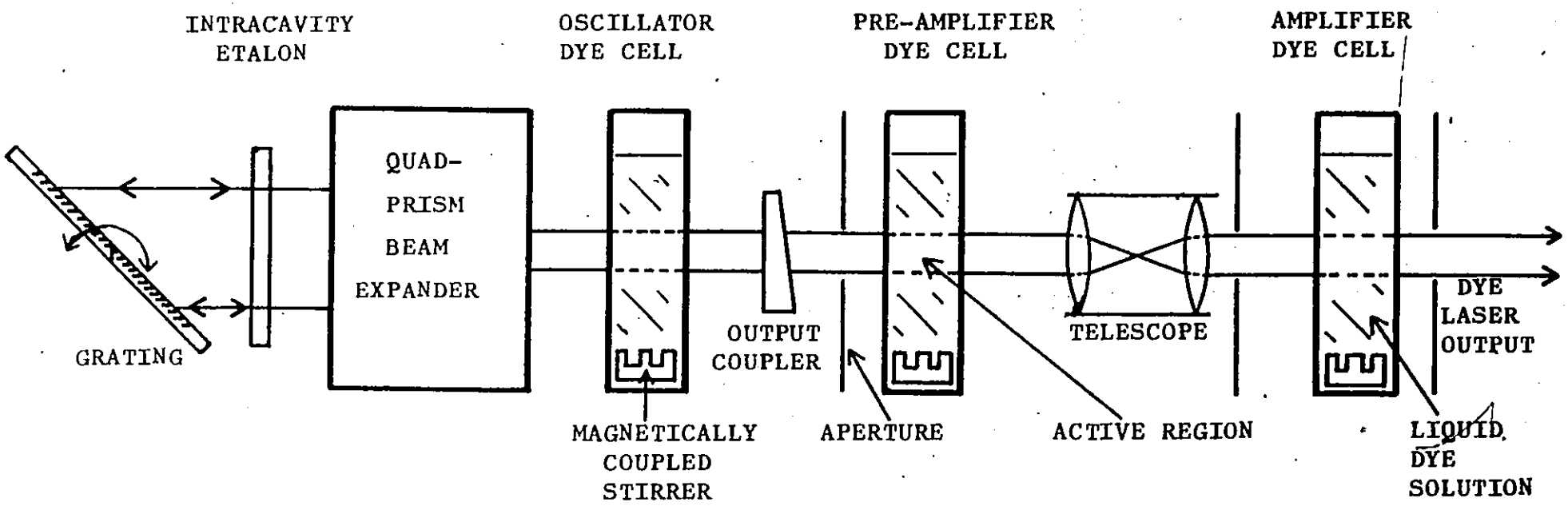

Figure 4- Schematic of the dye laser as used in this experiment for the Nd:YAG pump. The N_2 pumped dye laser used only the first two stages.

pumped by a nitrogen laser (both homemade) was used. The output pulses had a duration of 10ns and a repetition rate of 10Hz. A different F-P etalon (designed for blue wavelengths) was used to reduce the linewidth. Only a rough estimate of the linewidth could be achieved with the monitor etalon from Quanta-Ray (the only one available) due to the latter's poor performance at the 4640Å output of the laser. This was expected since the monitor etalon's working range was specified as 5400-7300Å. The linewidth estimate of 0.05-0.10 cm^{-1} was assumed more than adequate to resolve the 3D levels which are separated by 2.308 cm^{-1}. Subsequent experimentation proved this assumption valid. Output of this dye laser was typically 1-2 mJ per pulse.

The dyes used for the various levels in potassium along with their concentrations and solvents are shown in Table IV. The dyes were manufactured by Exciton Corporation. In most cases, the concentrations and solvents used were chosen following the recommendations given in the manufacturer's publication listing the available dyes.[32] For Oxazine 725 and the DCM/Oxazine 720 mixture, extensive experimentation had to be performed before a suitable output was achieved at the desired wavelength.

Approximately 2 cc of dye solution was placed in each of three cuvettes made by Precision Cells. It was circulated by a magnetically coupled, motor-driven stirrer.

The laser output was directed via two front-surface, aluminized mirrors into the entrance of the fluorescence cell. Since the beam had to travel about 8.8 meters to get to this point, beam divergence had increased the spot size to about 2 cm. in diameter. In order to achieve the requisite power densities for two-photon excitation, the beam was again collimated and also reduced in size to about 1 mm in diameter before entering the cell. The beam was reduced in size rather

than focussed so as to minimize the possibility of photo-ionization of the potassium atoms. This was accomplished by means of a second telescopic lens arrangement consisting of a 9 cm. diameter, 25 cm. focal length convex lens placed 27.7 cm. in front of a 1 cm. diameter, 2 cm. focal length convex lens. The latter was located 27 cm. from the center of the exit window of the fluorescence cell.

The fluorescence cell was a simple pyrex cylinder with two connecting glass arms. The top arm was connected to an external vacuum system with a base pressure of 1×10^{-7} Torr. This was achieved by using a Model ISC50B roughing pump and a Model E02 vapour diffusion pump (both manufactured by Edwards High Vacuum Ltd.) to evacuate the system initially. Then the vacuum system glassware was baked with Electrothermal heating tapes to about 160°C for two days while continuing evacuation. After removing these tapes, a cold trap situated between the pumps and the vacuum system was filled with liquid nitrogen.

Pressures were monitored at various stages of this procedure by a Consolidated Vacuum Corp. thermocouple gauge tube GTC-004 with gauge control unit GIC-110C for the low vacuum between the roughing pump and the diffusion pump (10-760 Torr), LKB gauge and control unit 3294B for the high vacuum after the diffusion pump (0.001-100 Torr) and the CVC ion gauge tube GIC-016 with the CVC GIC-110C control unit for the high vacuum (10^{-3}-10^{-8} Torr). The fluorescence cell could be closed off from the vacuum system by both greased (Apiezon N-grease), ground glass stopcocks and a greaseless, magnetically operated ground glass stopcock.

The bottom arm of the cell held about 1 gram of potassium which was distilled into the cell from a separate vacuum system (base pressure 2×10^{-7} Torr) using a previously sealed-in 5 gram ampoule of pure potassium supplied by Materials Ltd. Utmost care was taken to ensure that the potassium was as pure as

TABLE IV

Exciton Dyes Used in the Dye Lasers to Excite Potassium Energy Levels

Dye (Exciton Name)	Solvent	Concentration* (M)	Excited Levels	λ(Å)	Laser Pump
Coumarin 460	Ethanol	4.5×10^{-3}	$3D_{3/2}$	4643	N_2
			$3D_{5/2}$	4644	N_2
Oxazine 725	Methanol	1.0×10^{-3}	$4D_{3/2,5/2}$	7300	Nd
			$6S_{1/2}$	7286	
DCM/Oxazine 720	Methanol	$9\times10^{-4}/3\times10^{-4}$	$5D_{3/2,5/2}$	6626	Nd
			$7S_{1/2}$	6606	
DCM	Methanol	9.0×10^{-4}	$6D_{3/2,5/2}$	6310	Nd
			$8S_{1/2}$	6296	
Rhodamine 640	Methanol	5.3×10^{-4}	7D	6135	Nd
			$9S_{1/2}$	6126	
			8D	6028	
			$10S_{1/2}$	6021	
Rhodamine 640	Methanol	2.7×10^{-4}	9D	5957	Nd
			$11S_{1/2}$	5953	
Rhodamine 610	Methanol	5.0×10^{-4}	10D	5908	Nd
			$12S_{1/2}$	5905	
DPS	p-Dioxane	4.0×10^{-3}	$5P_{1/2}$	4048	N_2
			$5P_{3/2}$	4045	
PBD	Toluene/ Ethanol(1:1)	5.0×10^{-3}	$4D_{3/2}$	3650	N_2
			$4D_{5/2}$	3650	

* Concentrations shown are for those used in the oscillator and pre-amplifier stage dye cells. The dye in the amplifier dye cell was diluted by a factor of 2.

N_2- nitrogen laser pump Nd- Nd:YAG laser pump

possible, the only contamination being from air at a pressure of 2×10^{-7} Torr. The cell was transferred to the main vacuum system after sealing off the bottom arm attached to the distilling station. A breaker seal previously attached to the top arm could then be broken by a magnetically operated hammer after attaching the cell to the main system.

The stainless steel oven containing the cell was surrounded by six electrical heating strips wired in parallel which required about 1.8 Amps of current to maintain the contents at a temperature of 110°C. The oven was thickly insulated on all sides and then enclosed by an additional asbestos box, leaving openings for the vacuum arm and the entrance and exit pyrex windows for the exciting and fluorescent light.

A heating coil for the bottom arm of the cell kept the liquid potassium at a temperature of 90°C. When a lower temperature was desired for this potassium the heating coil was turned off and the oven's heating reduced by decreasing the supply current to 1.5 Amps to obtain temperatures of 70-72°C and 88-91°C for the potassium and the cell body respectively. The bottom arm was sufficiently insulated from the main body to account for this temperature difference. The main body was maintained at a higher temperature so as to prevent condensation of potassium vapour on the pyrex walls.

All temperatures given above were measured using copper-constantan thermocouples attached to the end of the bottom arm, to the joint of the bottom arm and the cell and to the upper main body of the cell by means of a ceramic paste. The voltage produced by the thermocouple against a room-temperature reference junction was measured with a Valhalla Scientific digital multimeter and converted to degrees Celsius using Leeds and Northrup conversion tables.

The entire oven assembly was surrounded by three sets of Helmholz coils (centered approximately on the excitation area

in the fluorescence cell) in order to cancel the earth's magnetic field in the vertical, east-west and north-south directions. Using an RFL Industries Model 101 magnetometer to measure the magnetic field strengths, the current in each pair of coils was adjusted to reduce the magnetic field in each of the three directions to less than 10^{-4} Gauss. Spurious magnetic fields produced by surrounding equipment and electrical lines could not be adjusted for.

Fluorescence from the cell was viewed at right angles to the exciting light in order to reduce the number of stray non-fluorescent photons entering the spectrometer. An opaque tube passed the fluorescent light from the exit window of the cell to an adjacent opaque box containing the detection equipment. A 9.5 cm. diameter, 9 cm. focal length convex lens focussed the fluorescence from the excitation area in the cell onto the entrance slit of a monochromator. In front of the monochromator were placed a polarizer (set at 54.7° to laser polarization to eliminate hyperfine quantum beats) and one of various colour glass filters. The filters were a Melles Griot 03-FCG-098 sharp cut-off filter and Ditrics Optics blue pass and red pass filters. These were used to reduce the amount of scattered laser light entering the monochromator.

The monochromator used was a Jarrell-Ash f/3.5 Model 82-410 with either 1 mm (bandwidth 30Å) or 0.1 mm (bandwidth 4Å) entrance and exit slits. It was calibrated using first a medium pressure mercury lamp (green and yellow lines), then a potassium Osram lamp in conjunction with transition wavelengths and intensities as given by Reference 33.

Another lens (4 cm. diameter, 4 cm. focal length) focussed the light from the exit slit onto an RCA C31034 photomultiplier tube in an air-cooled Pacific Photometrics Instruments Model 3457 tube housing. The tube was cooled to

about -20°C by means of a Peltier (Pacific Photometrics Instruments Model 33) cooler. The PMT was supplied by an Ortec 456 High Voltage power supply optimally set at -1800 volts. The PMT output was amplified with the Ortec 9301 fast pre-amplifier (powered by a Tennelec Model 3 NIMbin 12-volt supply) before being sent via a 60 cm., 50 ohm shielded coaxial cable with 50 ohm terminating shunt resistor to the Biomation Model 6500 Waveform recorder- a fast transient digitizer capable of time-resolving the PMT pulses in 1023 channels of 2,5 or 10 nanoseconds. The digitizer had previously been tested for linearity and time calibration[5] and found to be stable within 1 part in 10^7.

In order to trigger the digitizer to begin recording information after the passage of each laser pulse into the fluorescence cell, a photodiode was placed at the entrance to the cell to detect part of the laser pulse. Its output was then amplified and sent to the trigger source of the digitizer. Before it could be triggered, however, the digitizer had to be readied (armed) for the collection of data. For this purpose a PET-Commodore 2001-series microcomputer was connected to the digitizer in the 'handshake' manner. Using a machine language program, the computer was used to arm the digitizer and also to receive and store the digital information output from the digitizer once triggered. The time resolved fluorescence could be monitored from the digitizer by use of the X- and Y terminals of a Gould OS255 oscilloscope which were connected to the X and Y terminals of the digitizer.

The data, represented by counts per channel (one count per photon in most cases), was analysed by a non-linear Fortran program (written by P.C.Rogers of M.I.T) which fitted the data to an exponentially decaying curve (either equation 3 or 6 depending on the level excited) and calculated the lifetime (for one or two decay components) and its corresponding

statistical standard deviation (estimator of sigma). This could be checked with a linear least-squares fit computer program as applied to the natural logarithm of the raw data versus time.

PROCEDURE

In order to be able to easily adjust all of the optics for optimum fluorescence yield, one-photon excitation of the $5P_{1/2,3/2}$ levels was performed using the N_2 laser pump and the DPS dye. The mirrors were then adjusted to direct the dye laser output into the vertical center but to the far right of the horizontal center of the entrance window of the cell. This was to reduce possible radiation trapping. Then the first two lenses were positioned so that the laser beam passed through the center of each and also through the same spot in the entrance window as before.

After placing the proper filter in front of the monochromator the latter was set at about 7700Å to detect the $4P_{1/2}$-$4S_{1/2}$ cascade transition. The digitizer was set for +0.5 volt input, input offset of +0.96 and a 2ns time base per channel. The dye laser was adjusted to produce maximum fluorescence from the cell, and then the following adjustments were made to optimize the fluorescence signal:

a) Vertical position of the output lens of the telescope in front of the fluorescence cell (very critical)
b) Horizontal position of the lens in (a) (critical)
c) Vertical position of the fluorescence collection lens (very critical)
d) Horizontal position of the lens in (c)

The proper dye for the next level to be examined was then placed in the cuvettes of the desired dye laser and the diffraction grating adjusted for the approximately correct angle. While monitoring the PMT output with the monochromator using the 0.1 mm slits and set to detect the correct pump wavelength the wavelength of the dye laser was tuned using the grating angle adjustment until the detection system indicated (by a large PMT output) the desired wavelength. Neutral density filters were used to decrease the amount of laser light scattered into the detection system so as not to overload the PMT.

Once the approximate pump wavelength was achieved the monochromator could be reset to the correct transition wavelength ($nS_{1/2} \rightarrow 4P_{3/2}$, $nD_{3/2} \rightarrow 4P_{1/2}$ or $nD_{5/2} \rightarrow 4P_{3/2}$) and the oscilloscope monitored for the detection of fluorescence while the wavelength was adjusted again. When the pump wavelength was finally located the above parameters a)-d) were adjusted a second time in addition to the positioning of the dye cells and the focussing of the pump beams in the individual stages of the dye laser. Finally, the Fabry-Perot etalon in the oscillator cavity could be fine-tuned so that the proper level was being excited.

When a transition from a $nS_{1/2}$ level was being viewed the 1 mm slits could be used in the monochromator. However, since most $nD_{3/2} \rightarrow 4P_{1/2}$ and $nD_{5/2} \rightarrow 4P_{3/2}$ transitions were only separated by about 15Å, the 0.1 mm slits were used to view these transitions in order to achieve the proper resolution. Also a check could be made whether the $nD_{3/2}$ or $nD_{5/2}$ level was being excited since for the former two transitions (to $4P_{1/2}$ and to $4P_{3/2}$) could be distinguished while for the latter only the one to $4P_{3/2}$ was possible.

Due to the small energy separations of the D fine-structure levels and the bandwidth of the laser, the 7D to 10D levels could not be satisfactorily resolved. In these cases only the $nD_{3/2} \rightarrow 4P_{1/2}$ transition was viewed through the monochromator.

Prior to collection of the data, several tests were run to adjust for proper offset on the digitizer and to determine the effects of the Helmholz coils on the resulting data. Also it was desired to see the effect of the rate of fluorescence on the detection system. After exciting the $6D_{3/2}$ level, it was found that turning off or even reversing the current in the Helmholz coils had no discernible effect on the collected data (no Zeeman quantum beats were produced or resolved).

Nevertheless the proper magnetic field from the Helmholz coils was retained throughout the experiment.

It was discovered that too high a fluorescence yield could result in 'ringing' or after-pulsing in the photomultiplier tube. The electronics would then produce a damped oscillating waveform superimposed on the decay curve.[35] This was reduced substantially by changing from an older, slower (rise-time) Ortec timing filter amplifier to the much superior Ortec fast pre-amplifier which also reduced the background noise count and noise pickup.

Before each data collection run, the fluorescence cell was evacuated for about 15-30 minutes to remove any impurities. Then the cell was closed off from the vacuum system by closing the greaseless stopcock. The polarizer was placed in front of the filter in the detection system and adjusted for correct height and polarization angle.

Data collection times ranged from two hours for the $8S_{1/2}$ level to almost eighteen hours for the 10D and $12S_{1/2}$ levels. For the longer runs, the collection would be stopped every five or six hours to cool the laser, re-evacuate the fluorescence cell and replace the dye in the amplifier dye cell.

The temperature of the liquid potassium was kept at 90°C with the following exceptions:

a) $3D_{3/2,5/2}$ level (70°C)- since the $4P_{3/2} \rightarrow 4S_{1/2}$ transition was being viewed the temperature had to be reduced as much as was practical in order to minimize radiation trapping and still maintain a reasonable fluorescence yield.

b) $10D, 8S_{1/2}$ levels (72°C, 95°C, 120°C)- to test for the variation in lifetime with vapour pressure the lifetimes of these levels were measured over the temperature range shown.

c) $12S_{1/2}$- a third trial was performed for this level also when the laser system was set up to pump the 10D levels for a potassium temperature of 72°C.

The higher temperature (90°C) was used for most levels since it would produce a higher fluorescence yield, reducing collection times and background noise. Variations in lifetime were checked on only the most temperature and pressure sensitive levels.

Tests were also performed on the effect of the polarizer. When it was set at about 55° to the laser polarization the semi-log decay curves of the resulting data were linear and reasonably smooth. However, setting it at 35° or 0° or removing it entirely resulted in noticeable modulations in the decay curve, though not quite as pronounced as the theory predicted. These were definitely hyperfine quantum beats since the Zeeman quantum beats were already eliminated (or undetectable) and the fine-structure quantum beats, when present for the excitation of the 7D-10D levels, would be of too high a frequency to detect (about 12 GHz for the 10D level).

In most cases, the direct transition to the $4P_{1/2}$ or $4P_{3/2}$ level was viewed. For the $4D_{3/2,5/2}$ and $6S_{1/2}$ levels problems arose. There was a relatively high fluorescence yield when the $6S_{1/2}$ level was excited. But upon adjusting to the correct pump wavelength for the 4D levels (the same dye was used) almost no fluorescence was detected which could be distinguished from the background noise (about 1 or 2 counts every 20 seconds). It was discovered (both experimentally and theoretically) that the oscillator strength of the 4P→4D transition was far too small to populate either 4D level by two-photon excitation. In addition the branching ratios for the 4D→4P transitions are insignificant compared to the

4D→5P branching ratios. Even so, no fluorescence could be detected which was distinguishable from noise when viewing the $5P_{3/2} \rightarrow 4S_{1/2}$ cascade transition from the 4D levels.

An attempt was made at quadrupole excitation of the 4D levels using the PBD dye at 3650Å and pumped by the N_2 laser without success due to several limitations of the equipment. Ideally, quartz optics should have been used for the entire system, including the laser and the windows of the fluorescence cell but excluding the detection system, but these were not available at the time. It was also difficult to adjust the laser without the use of an ultraviolet photodetector since the laser output was invisible to the naked eye.

A second problem surfaced when it was found that the wavelength necessary to excite the $6S_{1/2}$ level (7286Å) and the viewed direct transition (6911Å) were close enough to cause significant invasion of laser scatter into the spectrometer because of a lack of proper bandpass filters or interference filters and despite the use of the monochromator. Though some of this data was good a check was performed by viewing the $5P_{3/2} \rightarrow 4S_{1/2}$ cascade transition and analysing the resulting data for two decay components. No significant difference was found in the results of the two methods.

As stated previously it was necessary to view the cascade transition from the $4P_{3/2}$ level when the 3D levels were excited since the direct transition photons could not be detected.

Analysis of the data was carried out on those channels comprising about 3 to 5 lifetimes for the level concerned, leaving out the first 10-150 channels which might be affected by laser scatter or after-pulsing effects and noise pickup and also eliminating any of the last 10-100 channels where noise intrusion was evident. The computer program used for this analysis was tested on theoretical decay curves

involving one or two decay components. In the case of one decay component the program was found to be accurate to within 1 part in 10^5. It was slightly less accurate in analysing for two decay components except when the lifetimes being measured were fairly close to each other (within about 50% of the smaller lifetime). Then the program would tend to self-destruct unless the entire decay curve were analysed such that the initial channel showed 0 counts. In other words the curve being analysed must look exactly like the theoretical decay curve starting at time zero.

RESULTS AND DISCUSSION

The results of this investigation into the lifetimes of some S and D states of potassium are presented in Table V. These results are averages over two sets of data for each level (in some cases 3 or 4 sets of data). In all cases the error was taken as twice the statistical standard deviation of the lifetime (2σ) as calculated by the computer program. Representative examples of the data obtained can be seen in the semi-logarithmic plots shown in Figures 5-10.

Both the 10D and $8S_{1/2}$ levels' lifetimes were measured at potassium temperatures of 72°C, 95°C and 120°C with no systematic variation appearing in the resulting lifetimes. The lifetime of the $12S_{1/2}$ level was measured at a potassium temperature of 72°C in addition to the previous measurement at 90°C with no significant difference between the two values. Thus it can be concluded that the collisional depopulation rates were insignificant or at least less than the statistical standard deviations of the data.

The radiation trapping effects were very significant in the cascade transition $4P_{3/2} \rightarrow 4S_{1/2}$ when the 3D levels were being excited at potassium temperatures above 80°C. However, no change was found in the decay curve for the fluorescence signal when the temperature was decreased from 75°C to 70°C. It was assumed that radiation trapping effects had been minimized at this point. Thus, the analysed data for the $3D_{3/2}$ level would appear as in Figure 9. If the temperature were decreased beyond 70°C it was found that the fluorescence signal decreased in intensity so much that virtually all the light being detected was from laser scatter.

Some of the results for the investigation of hyperfine quantum beats can be seen in Figures 11 and 12. The first shows the experimental and theoretical plots for the decay curve of the fluorescence intensity from the direct transition out of the $6D_{3/2}$ level to the $4P_{1/2}$ level when the polarizer

TABLE V

Results of This Investigation

Lifetimes of Excited S and D States of Potassium

1. Excited level populated by two-photon absorption:

Level	Lifetime (ns)
$6S_{1/2}$	87.9±3.5
$7S_{1/2}$	155 ± 6
$8S_{1/2}$	238 ± 4
$9S_{1/2}$	384 ± 14
$10S_{1/2}$	575 ± 26
$11S_{1/2}$	783 ± 50
$12S_{1/2}$	1148 ± 42
$5D_{3/2}$	572 ± 14
$5D_{5/2}$	553 ± 16
$6D_{3/2}$	807 ± 20
$6D_{5/2}$	792 ± 12
7D	1201 ± 26
8D	1533 ± 80
9D	2000 ± 140
10D	2268 ± 46

2. Excited level populated by single-photon, quadrupole absorption:

Level	Lifetime (ns)
$3D_{3/2}(4P_{3/2})$	42±3(28±1)
$3D_{5/2}(4P_{3/2})$	42±3(28±1)

DATA SETS

The following seven figures are representative samples of the data that was accumulated for the fluorescence from various transitions in potassium. The data is illustrated by a semi-logarithmic graph of the counts per channel versus the time elapsed since the beginning of the laser pulse. In each case the polarizer was set at $\theta_d = 55^\circ$ except as noted in Figure 12. The temperature of the potassium for each measurement was 90° C except for:

Figures 8 and 9- 72° C

Figure 10- 70° C

Also for Figure 10 there is a slight delay of about 80 nanoseconds between the beginning of the laser pulse and the time at which the Biomation digitizer began accumulating data from the fluorescence signal.

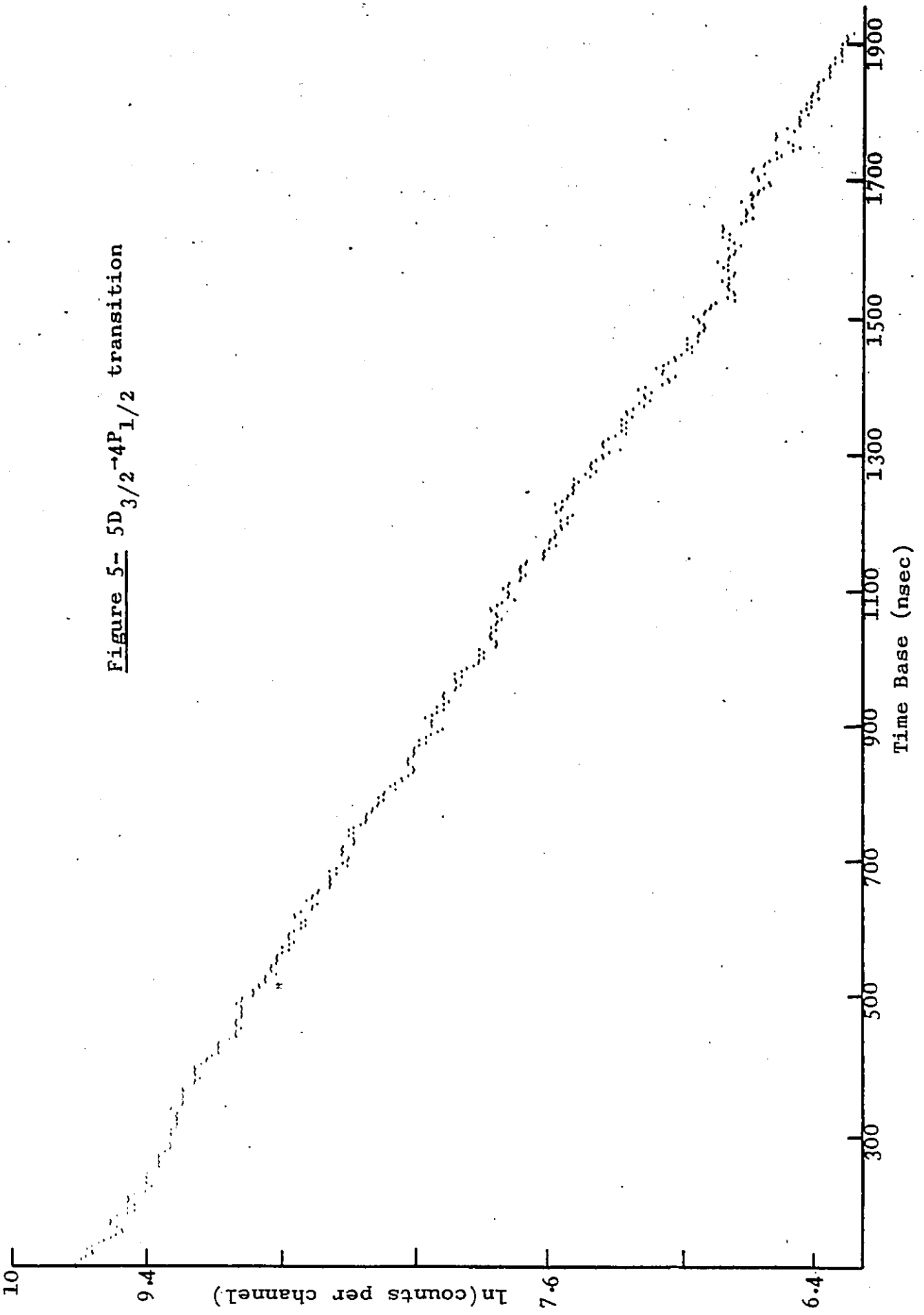

Figure 5- $5D_{3/2} \rightarrow 4P_{1/2}$ transition

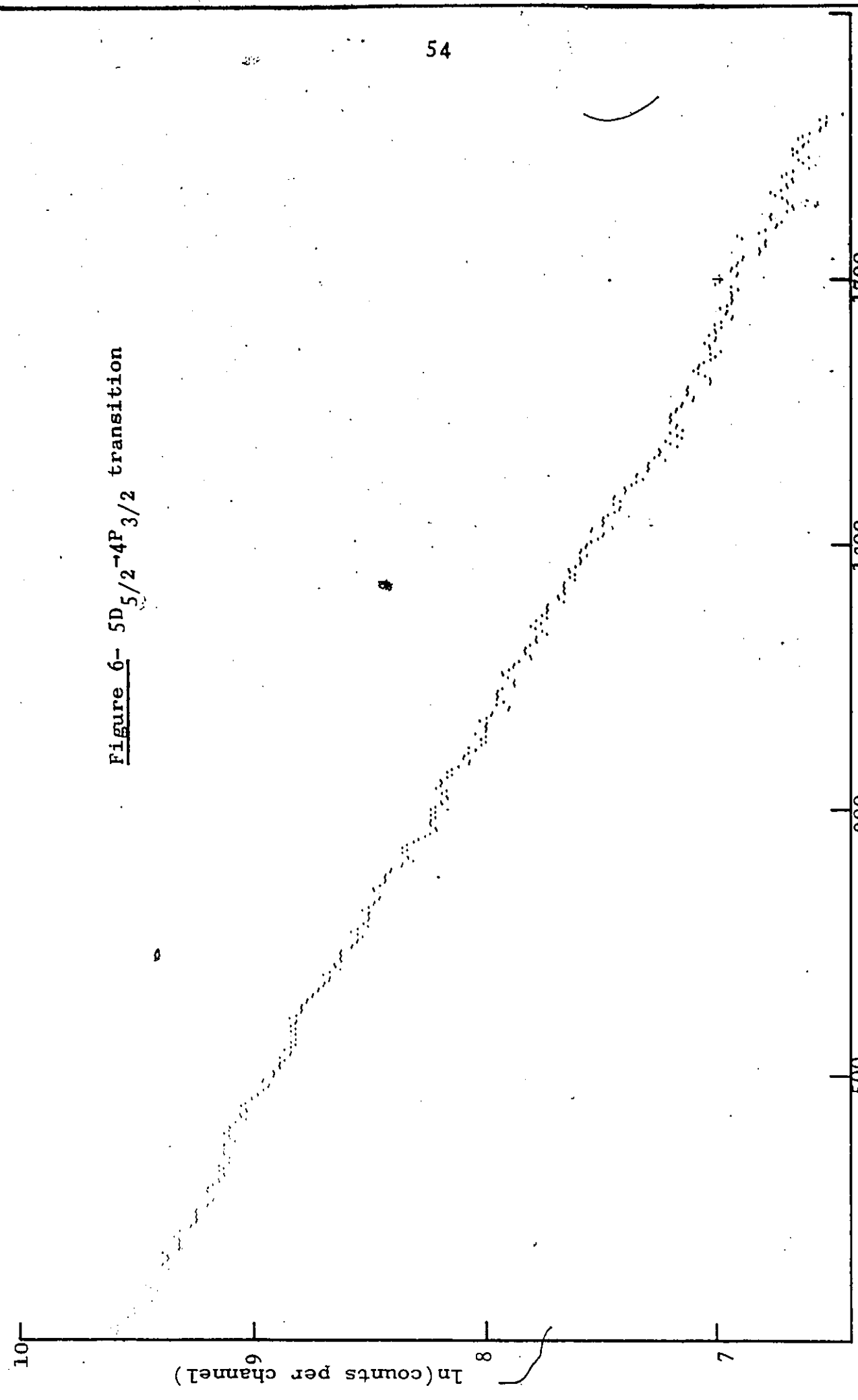

Figure 6- $5D_{5/2}-4P_{3/2}$ transition

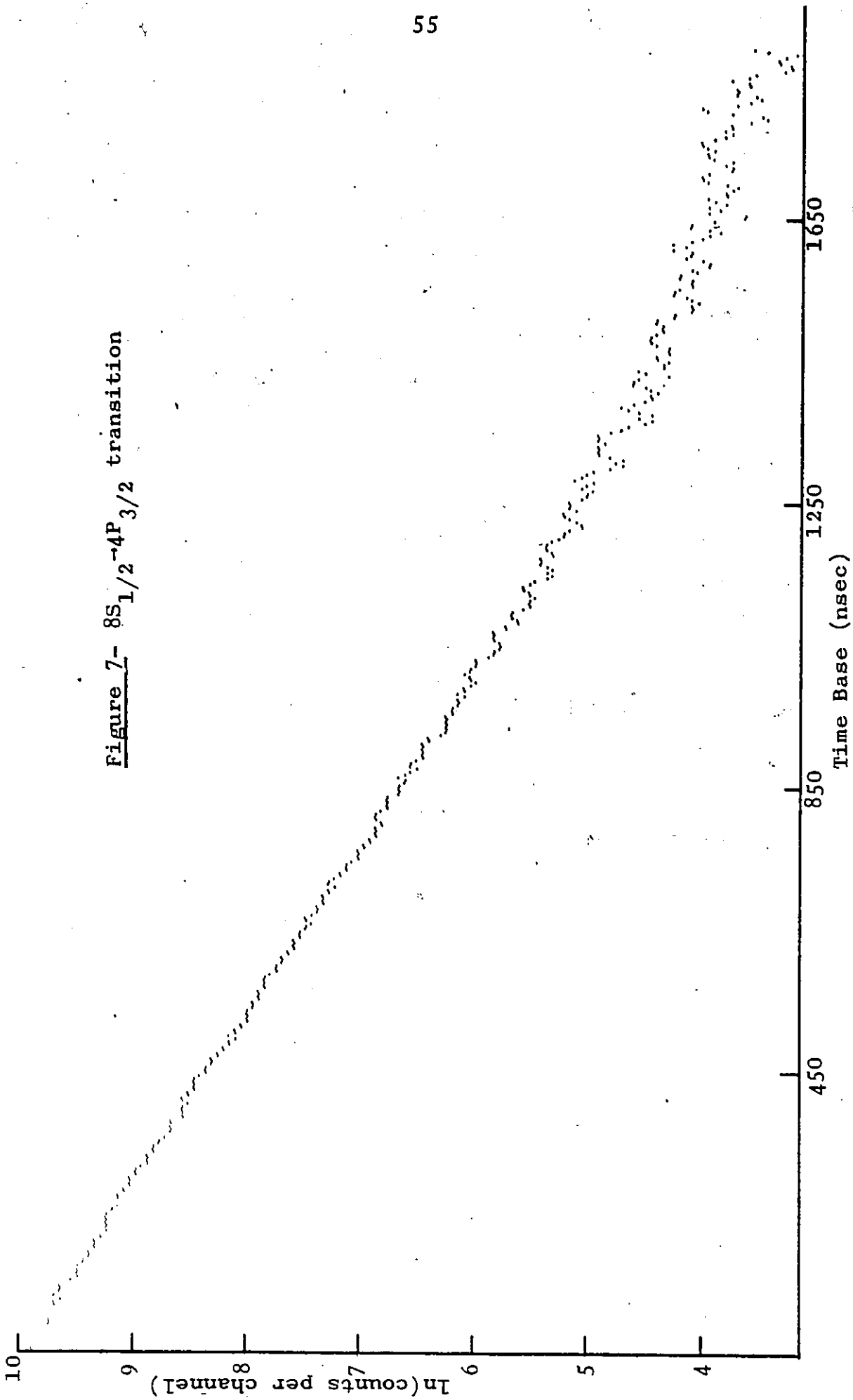

Figure 7- $8S_{1/2}-4P_{3/2}$ transition

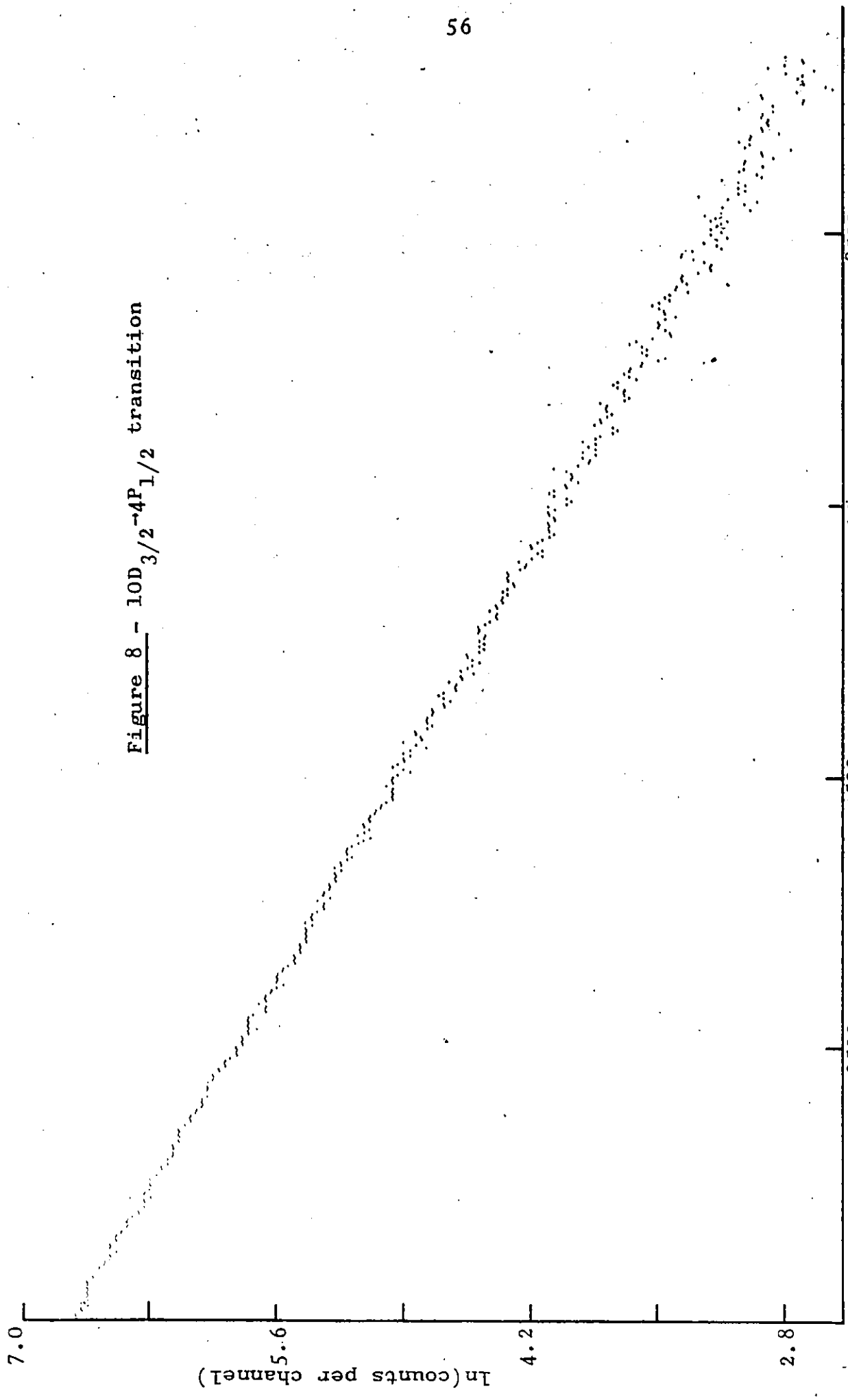

Figure 8 - $10D_{3/2} \rightarrow 4P_{1/2}$ transition

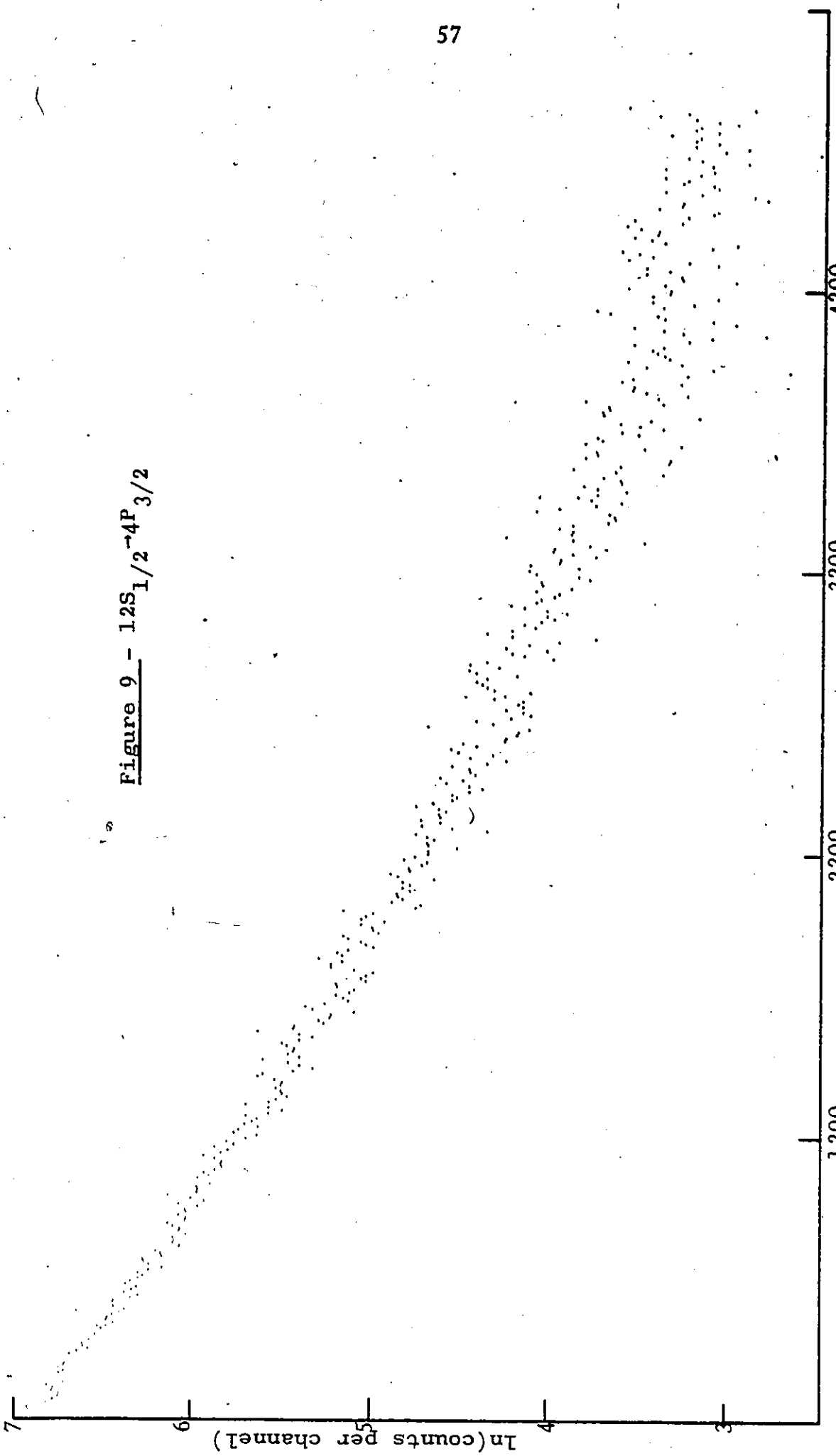

Figure 9 - $12S_{1/2} \rightarrow 4P_{3/2}$

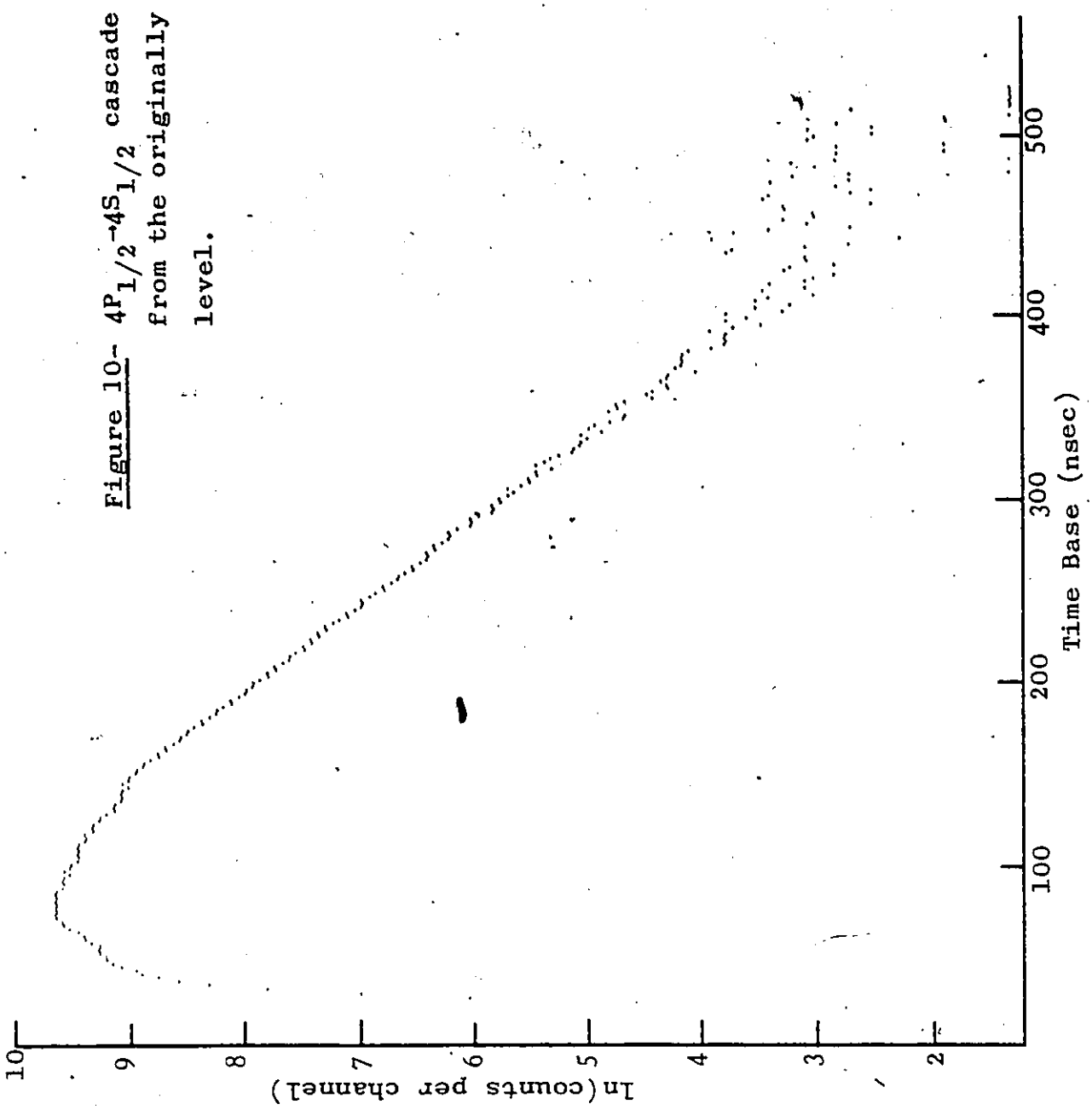

Figure 10- $4P_{1/2} \rightarrow 4S_{1/2}$ cascade transition from the originally excited $3D_{3/2}$ level.

has been set at ~55° to the linearly polarized laser light. The second figure shows the comparison for the polarizer set at ~35°. For the theoretical plot the magnetic coupling constant as given in Reference 31 (0.2 ± 0.2 MHz) was used. No more accurate value was available.

It is obvious that the quantum beats have been eliminated in the first figure in both plots showing good agreement between theory and experiment. In the second figure there is a marked disagreement after the first few hundred nanoseconds. Pendrill and Series[30] have shown that the quantum beats are strongly damped due to collisional mixing amongst the hyperfine levels which is what the experimental plot in Figure 11 shows. The theoretical plot, however, has not taken this into account. In addition the latter is based upon a very inaccurate measurement of the magnetic dipole coupling constant for the $6D_{3/2}$ level of potassium.

The lifetimes for the levels of potassium as measured here are compared to both the theoretical results as derived earlier in this dissertation (including BBR effects) and to the only other experimental results (if any) in Table VI. There is quite good agreement in all cases except possibly for the $6D_{3/2}$ and $6D_{5/2}$ levels. A better comparison can be seen in Figures 13 and 14 where the logarithm of the lifetime in nanoseconds has been plotted versus the logarithm of n* for the $nS_{1/2}$ and $nD_{3/2}$ levels respectively. In both graphs the experimental values from Table V are compared to both the natural radiative lifetimes and the BBR reduced theoretical lifetimes from Table III. The agreement appears to be better between the experimental and the BBR reduced theoretical lifetimes. Some slight discrepancies can be explained by the fact that the BBR reduced lifetimes were calculated for a 300°K temperature while the experiment used 349°K or 367°K.

If the levels for which the lifetimes are being measured

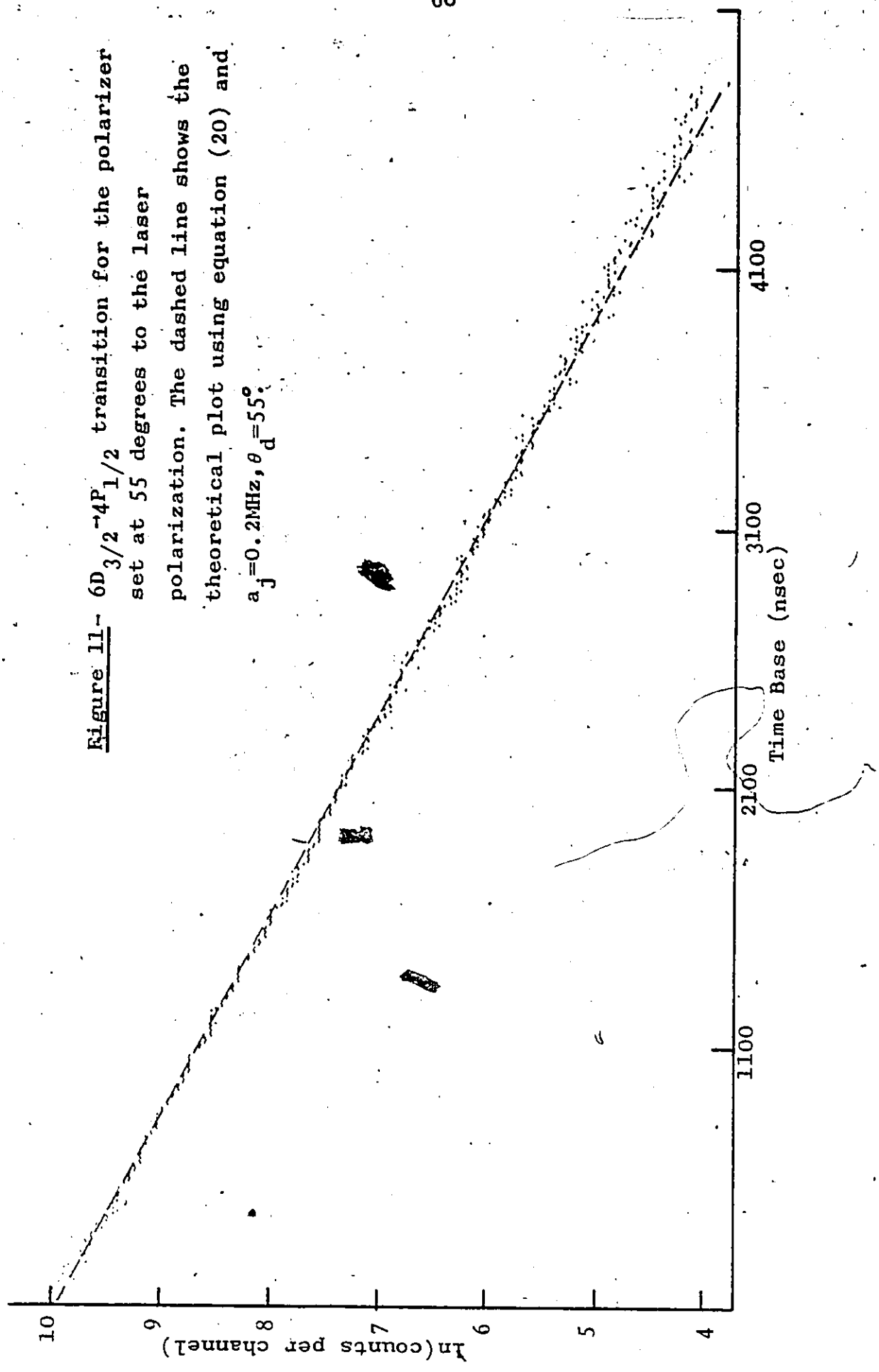

Figure 11- $6D_{3/2}-4P_{1/2}$ transition for the polarizer set at 55 degrees to the laser polarization. The dashed line shows the theoretical plot using equation (20) and $a_j=0.2MHz, \theta_d=55°$.

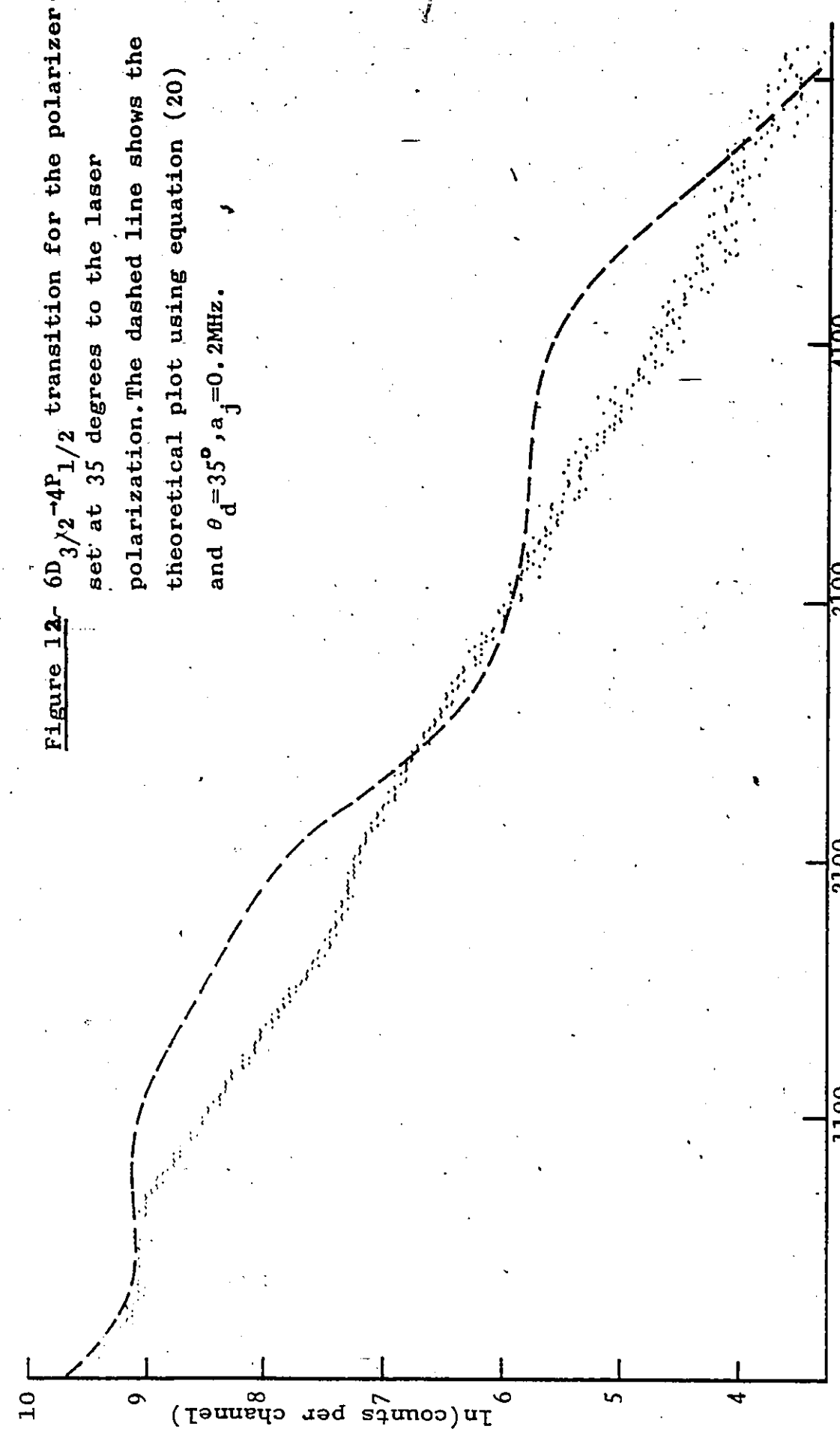

Figure 12- $6D_{3/2}\rightarrow 4P_{1/2}$ transition for the polarizer set at 35 degrees to the laser polarization. The dashed line shows the theoretical plot using equation (20) and $\theta_d = 35°$, $a_j = 0.2$MHz.

TABLE VI

A Comparison of Experimental and Theoretical Results For the Lifetimes of S and D States of Potassium

Level	This Investigation	Other Experiments[28]	Theoretical
$6S_{1/2}$	87.9±3.5	68 ± 9[10]	87.7
$7S_{1/2}$	155 ± 6	165 ± 12	157
$8S_{1/2}$	238 ± 4	260 ± 14	260
$9S_{1/2}$	384 ± 14	441 ± 18	398
$10S_{1/2}$	575 ± 26	600 ± 130	575
$11S_{1/2}$	783 ± 50	910 ± 120	796
$12S_{1/2}$	1148 ± 42	---------	1062
$5D_{3/2}$	572 ± 14	---------	572
$5D_{5/2}$	553 ± 16	610 ± 90	529
$6D_{3/2}$	807 ± 20	--------	1036
$6D_{5/2}$	792 ± 12	890 ± 60	1047
$7D_{3/2}$	1201 ± 26	--------	1291
$7D_{5/2}$	---------	1210 ± 100	1249
$8D_{3/2}$	1533 ± 80	----------	1553
$8D_{5/2}$	---------	1590 ± 130	1540
$9D_{3/2}$	2000 ± 140	----------	1866
$9D_{5/2}$	----------	2040 ± 300	1914
$10D_{3/2}$	2268 ± 46	----------	2353
$10D_{5/2}$	---------	----------	2319
$3D_{3/2}$ ($4P_{3/2}$)	42±3(28±1)	41±3[4](27.6±0.8)[6]	38.5(26.9)
$3D_{5/2}$ ($4P_{3/2}$)	42±3(28±1)	41±3 (27.6±0.8)	38.9(26.9)

can be described accurately by hydrogenic wavefunctions these plots would then be linear and have slopes of 3 (that is $\tau \sim n^{*3}$). For the $S_{1/2}$ levels this is not quite true since the experimental and BBR reduced lifetimes' plots for potassium have slopes of 2.7 ± 0.1 and 2.6 ± 0.1 respectively. It is apparent, though, that the plots for the $nD_{3/2}$ lifetimes are only linear for $n \geq 5$ but with slopes of 2.0 ± 0.1 and 1.9 ± 0.1 for the experimental and BBR reduced lifetime plots respectively. This would indicate that hydrogenic wavefunctions should not be used to describe the D levels of potassium.

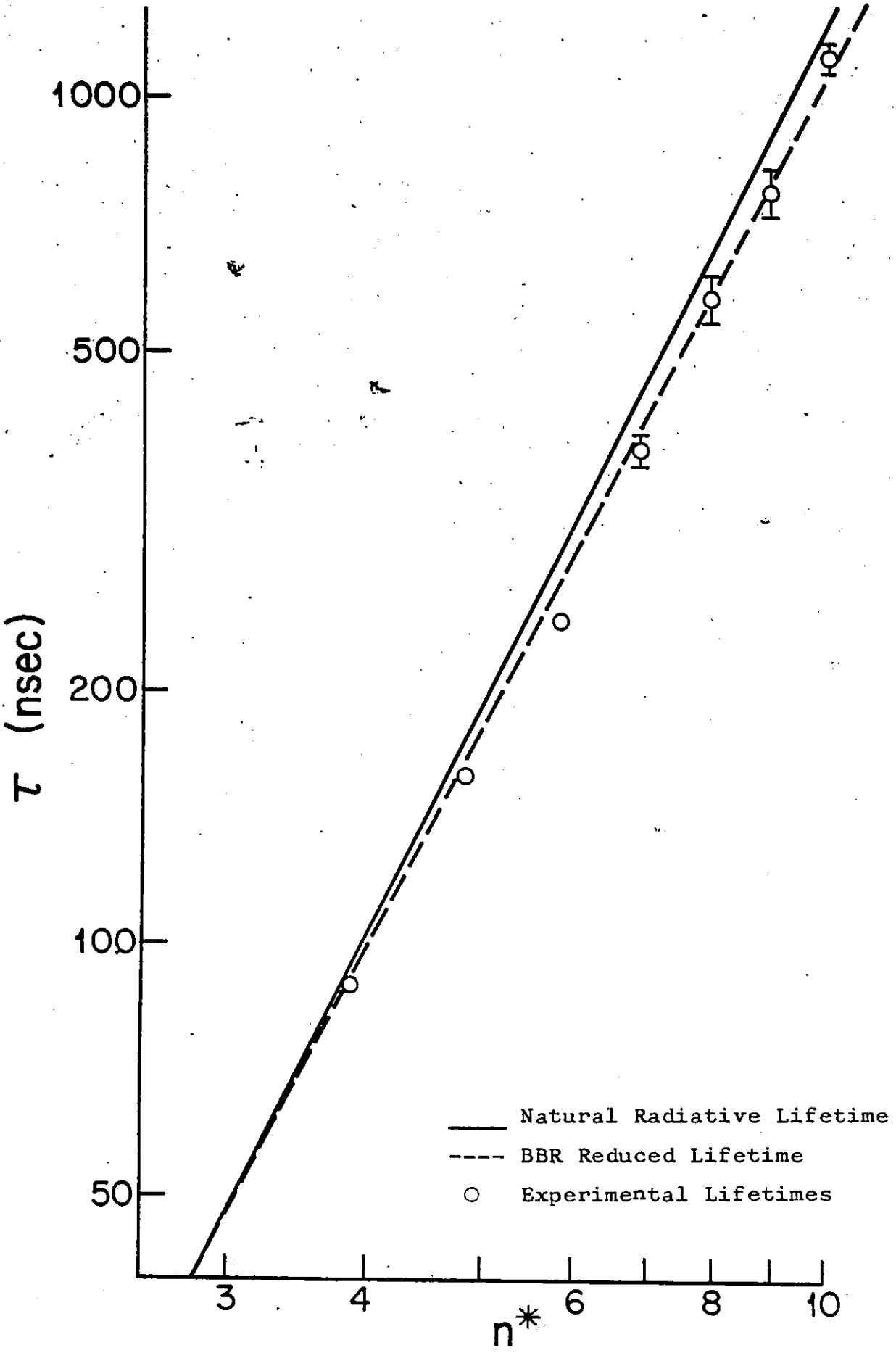

Figure 13- The Log-Log graph of lifetime versus n* for the $nS_{1/2}$ levels of potassium

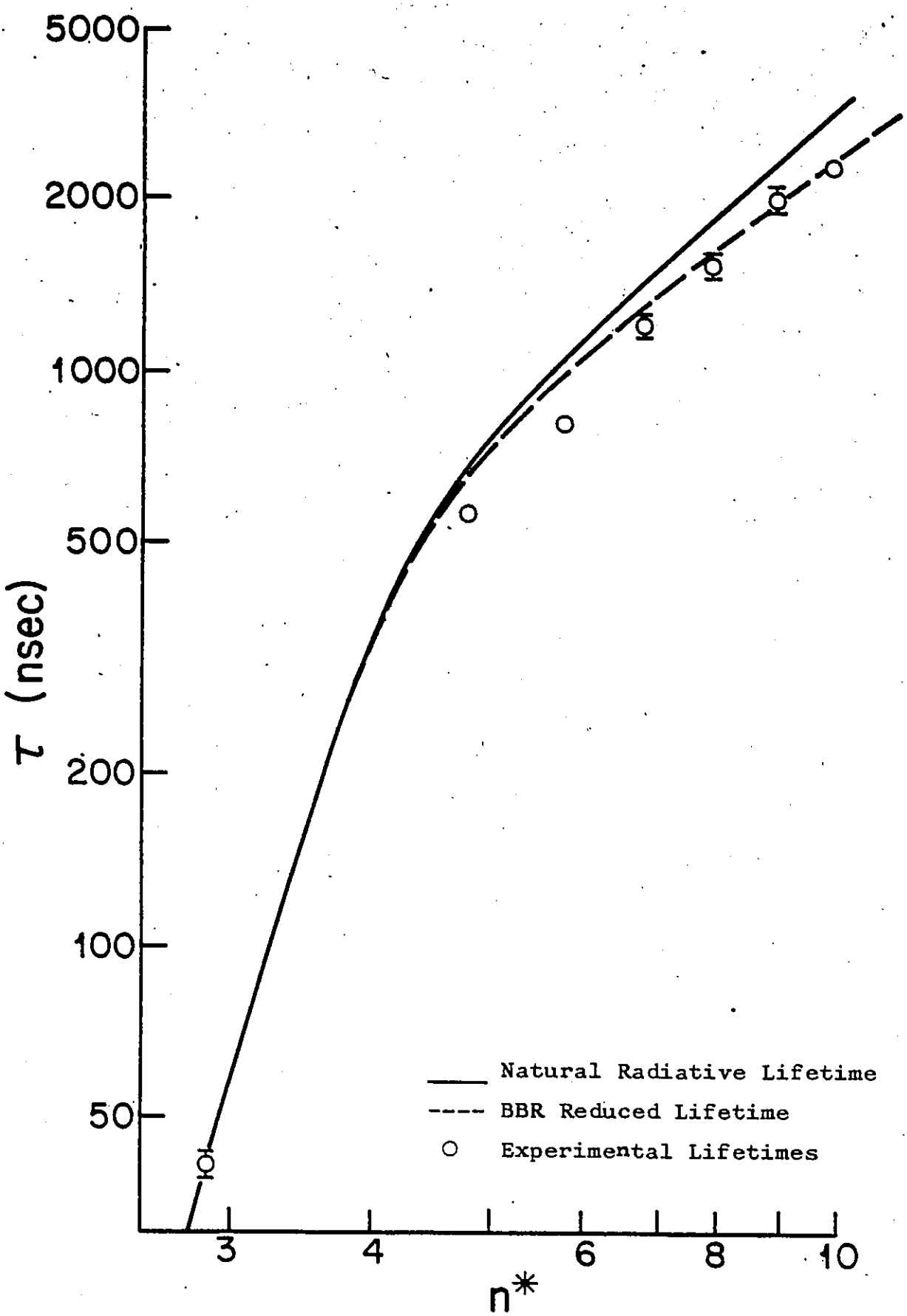

Figure 14- The Log-Log graph of lifetime versus n* for the $nD_{3/2}$ levels of potassium.

CONCLUSIONS

Even though the experimentally measured lifetimes and the theoretically calculated lifetimes matched to within experimental error in most cases, the natural radiative lifetimes were not determined. In order to do this it would be necessary to take lifetime measurements at varying temperatures for the potassium for each level so as to be able to extrapolate to a 0°K temperature. Also one would have to ensure that none of the experimental temperatures were high enough to make collisional depopulation significant.

From the results of the three D states' lifetimes whose fine-structure could be resolved it cannot be concluded that there is a difference in lifetimes between the two fine-structure levels although the theory would seem to predict such a difference. This is due in part to the very small separation of these levels and to the insufficient time allowed to collect a suitable amount of data for each level. Collection times would have to be increased by a factor of 5-10 for this particular atom so as to accurately determine the difference, if any, in the lifetimes of the $nD_{3/2}$ and $nD_{5/2}$ levels.

APPENDICES

APPENDIX A

Transition Probabilities for K I

The following A coefficients were calculated by the author using the Warner method as described previously. (N.B. 6.899(6) = 6.899×10^6)

I) S Levels

Transition		$A(s^{-1})$
Initial Level	Final Level	
$5S_{1/2}$	$4P_{1/2}$	6.899(6)
	$4P_{3/2}$	1.381(7)
$6S_{1/2}$	$4P_{1/2}$	2.256(6)
	$4P_{3/2}$	4.498(6)
	$5P_{1/2}$	1.558(6)
	$5P_{3/2}$	3.087(6)
$7S_{1/2}$	$4P_{1/2}$	1.081(6)
	$4P_{3/2}$	2.153(6)
	$5P_{1/2}$	5.512(5)
	$5P_{3/2}$	1.087(6)
	$6P_{1/2}$	4.883(5)
	$6P_{3/2}$	9.680(5)
$8S_{1/2}$	$4P_{1/2}$	6.045(5)
	$4P_{3/2}$	1.204(6)
	$5P_{1/2}$	2.885(5)
	$5P_{3/2}$	5.687(5)
	$6P_{1/2}$	1.849(5)
	$6P_{3/2}$	3.645(5)
	$7P_{1/2}$	1.898(5)
	$7P_{3/2}$	3.762(5)
$9S_{1/2}$	$4P_{1/2}$	3.728(5)
	$4P_{3/2}$	7.425(5)

Transition		A(s^{-1})
Initial Level	Final Level	
$9S_{1/2}$	$5P_{1/2}$	1.730(5)
	$5P_{3/2}$	3.410(5)
	$6P_{1/2}$	1.032(5)
	$6P_{3/2}$	2.033(5)
	$7P_{1/2}$	7.546(4)
	$7P_{3/2}$	1.487(5)
	$8P_{1/2}$	8.558(4)
	$8P_{3/2}$	1.697(5)
$10S_{1/2}$	$4P_{1/2}$	2.462(5)
	$4P_{3/2}$	4.903(5)
	$5P_{1/2}$	1.126(5)
	$5P_{3/2}$	2.218(5)
	$6P_{1/2}$	6.513(4)
	$6P_{3/2}$	1.282(5)
	$7P_{1/2}$	4.417(4)
	$7P_{3/2}$	8.692(4)
	$8P_{1/2}$	3.529(4)
	$8P_{3/2}$	6.950(4)
	$9P_{1/2}$	4.304(4)
	$9P_{3/2}$	8.530(4)
$11S_{1/2}$	$4P_{1/2}$	1.711(5)
	$4P_{3/2}$	3.407(5)
	$5P_{1/2}$	7.750(4)
	$5P_{3/2}$	1.527(5)
	$6P_{1/2}$	4.411(4)
	$6P_{3/2}$	8.686(4)
	$7P_{1/2}$	2.896(4)
	$7P_{3/2}$	5.699(4)
	$8P_{1/2}$	2.144(4)
	$8P_{3/2}$	4.210(4)

Transition		$A(s^{-1})$
Initial Level	Final Level	
$11S_{1/2}$	$9P_{1/2}$	1.821(4)
	$9P_{3/2}$	3.591(4)
	$10P_{1/2}$	2.349(4)
	$10P_{3/2}$	4.653(4)
$12S_{1/2}$	$4P_{1/2}$	1.237(5)
	$4P_{3/2}$	2.464(5)
	$5P_{1/2}$	5.571(4)
	$5P_{3/2}$	1.115(5)
	$6P_{1/2}$	3.140(4)
	$6P_{3/2}$	6.224(4)
	$7P_{1/2}$	2.022(4)
	$7P_{3/2}$	4.007(4)
	$8P_{1/2}$	1.459(4)
	$8P_{3/2}$	2.845(4)
	$9P_{1/2}$	1.131(4)
	$9P_{3/2}$	2.166(4)
	$10P_{1/2}$	1.068(4)
	$10P_{3/2}$	2.074(4)
	$11P_{1/2}$	1.380(4)
	$11P_{3/2}$	2.736(4)

II) D Levels

Transition Initial Level	Final Level	$A(s^{-1})$ J=3/2	$A(s^{-1})$ J=5/2
$3D_J$	$4P_{1/2}$	2.171(7)	--
	$4P_{3/2}$	4.269(6)	2.569(7)
$4D_J$	$4P_{1/2}$	1.555(3)	--
	$4P_{3/2}$	8.960(2)	5.909(3)
	$5P_{1/2}$	2.974(6)	--
	$5P_{3/2}$	5.868(5)	3.538(6)
$5D_J$	$4P_{1/2}$	4.540(5)	--
	$4P_{3/2}$	1.178(5)	7.302(5)
	$5P_{1/2}$	3.777(4)	--
	$5P_{3/2}$	7.113(3)	4.185(4)
	$6P_{1/2}$	7.225(5)	--
	$6P_{3/2}$	1.424(5)	8.534(5)
	$4F_{5/2}$	2.464(5)	1.174(4)
	$4F_{7/2}$	--	2.349(5)
$6D_J$	$4P_{1/2}$	2.732(5)	--
	$4P_{3/2}$	5.102(4)	3.166(5)
	$5P_{1/2}$	2.100(1)	--
	$5P_{3/2}$	8.000(0)	5.800(1)
	$6P_{1/2}$	3.323(4)	--
	$6P_{3/2}$	6.256(3)	3.754(4)
	$7P_{1/2}$	2.402(5)	--
	$7P_{3/2}$	4.732(4)	2.863(5)
	$4F_{5/2}$	1.030(5)	4.909(3)
	$4F_{7/2}$	--	9.818(4)
	$5F_{5/2}$	1.672(5)	7.969(3)
	$5F_{7/2}$	--	1.594(5)

Transition Initial Level	Final Level	$A(s^{-1})$ J=3/2	$A(s^{-1})$ J=5/2
$7D_J$	$4P_{1/2}$	2.451(5)	--
	$4P_{3/2}$	8.045(4)	3.638(5)
	$5P_{1/2}$	1.440(4)	--
	$5P_{3/2}$	3.005(3)	7.029(3)
	$6P_{1/2}$	2.510(2)	--
	$6P_{3/2}$	4.400(1)	2.410(2)
	$7P_{1/2}$	1.839(4)	--
	$7P_{3/2}$	3.473(3)	2.095(4)
	$8P_{1/2}$	9.767(4)	--
	$8P_{3/2}$	1.924(4)	1.165(5)
	$4F_{5/2}$	5.491(4)	2.616(3)
	$4F_{7/2}$	--	5.232(4)
	$5F_{5/2}$	7.786(4)	3.709(3)
	$5F_{7/2}$	--	7.418(4)
	$6F_{5/2}$	9.802(4)	4.670(3)
	$6F_{7/2}$	--	9.339(4)
$8D_J$	$4P_{1/2}$	2.598(5)	--
	$4P_{3/2}$	5.258(4)	3.180(5)
	$5P_{1/2}$	6.773(3)	--
	$5P_{3/2}$	1.477(3)	8.972(3)
	$6P_{1/2}$	4.400(1)	--
	$6P_{3/2}$	2.600(1)	1.670(2)
	$7P_{1/2}$	2.032(3)	--
	$7P_{3/2}$	3.660(2)	2.178(3)
	$8P_{1/2}$	9.997(3)	--
	$8P_{3/2}$	1.894(3)	1.143(4)
	$9P_{1/2}$	4.563(4)	--
	$9P_{3/2}$	8.984(3)	5.448(4)
	$4F_{5/2}$	3.323(4)	1.583(3)
	$4F_{7/2}$	--	3.166(4)

Transition Initial Level	Final Level	A (s^{-1}) J=3/2	A(s^{-1}) J=5/2
$8D_J$	$5F_{5/2}$	4.459(4)	2.124(3)
	$5F_{7/2}$	--	4.249(4)
	$6F_{5/2}$	4.923(4)	2.345(3)
	$6F_{7/2}$	--	4.691(4)
	$7F_{5/2}$	5.736(4)	2.733(3)
	$7F_{7/2}$	--	5.466(4)
$9D_J$	$4P_{1/2}$	2.128(5)	--
	$4P_{3/2}$	4.313(4)	2.603(5)
	$5P_{1/2}$	1.683(4)	--
	$5P_{3/2}$	8.640(3)	7.833(3)
	$6P_{1/2}$	8.980(2)	--
	$6P_{3/2}$	2.170(2)	1/332(3)
	$7P_{1/2}$	4.300(1)	--
	$7P_{3/2}$	7.000(0)	3.800(1)
	$8P_{1/2}$	1.981(3)	--
	$8P_{3/2}$	3.630(2)	2.178(3)
	$9P_{1/2}$	5.629(3)	--
	$9P_{3/2}$	1.075(3)	6[illegible]88(3)
	$10P_{1/2}$	2.358(4)	--
	$10P_{3/2}$	4.644(3)	2.819(4)
	$4F_{5/2}$	2.181(4)	1.039(3)
	$4F_{7/2}$	--	2.078(4)
	$5F_{5/2}$	2.839(4)	1.352(3)
	$5F_{7/2}$	--	2.705(4)
	$6F_{5/2}$	2.978(4)	1.419(3)
	$6F_{7/2}$	--	2.837(4)
	$7F_{5/2}$	3.047(4)	1.451(3)
	$7F_{7/2}$	--	2.902(4)
	$8F_{5/2}$	3.456(4)	1.647(3)
	$8F_{7/2}$	--	3.293(4)

Transition		$A(s^{-1})$	$A(s^{-1})$
Initial Level	Final Level	J=3/2	J=5/2
$10D_J$	$4P_{1/2}$	1.723(5)	--
	$4P_{3/2}$	3.494(4)	2.109(5)
	$5P_{1/2}$	5.991(3)	--
	$5P_{3/2}$	4.530(3)	1.330(4)
	$6P_{1/2}$	1.587(3)	--
	$6P_{3/2}$	3.500(2)	2.123(3)
	$7P_{1/2}$	5.000(0)	--
	$7P_{3/2}$	<1(-2)	<1(-1)
	$8P_{1/2}$	3.910(2)	--
	$8P_{3/2}$	6.800(1)	4.090(2)
	$9P_{1/2}$	1.454(3)	--
	$9P_{3/2}$	2.680(2)	1.615(3)
	$10P_{1/2}$	3.387(3)	--
	$10P_{3/2}$	6.580(2)	4.080(3)
	$11P_{1/2}$	1.320(4)	--
	$11P_{3/2}$	2.638(3)	1.569(4)
	$4F_{5/2}$	1.516(4)	7.220(2)
	$4F_{7/2}$	--	1.444(4)
	$5F_{5/2}$	1.938(4)	9.220(2)
	$5F_{7/2}$	--	1.844(4)
	$6F_{5/2}$	1.975(4)	9.410(2)
	$6F_{7/2}$	--	1.881(4)
	$7F_{5/2}$	1.929(4)	9.170(2)
	$7F_{7/2}$	--	1.834(4)
	$8F_{5/2}$	1.913(4)	9.070(2)
	$8F_{7/2}$	--	1.814(4)
	$9F_{5/2}$	2.165(4)	1.028(3)
	$9F_{7/2}$	--	2.056(4)

N.B.- $1.735(5) = 1.735 \times 10^5$

APPENDIX B

The following is a derivation for the coefficient $A_{k_i q_i k_{i-1} q_{i-1}}^{F_i F_i' F_{i-1} F_{i-1}'}(Q_i)$ as defined by Silverman et al. but calculated here for hyperfine quantum beats.

As stated in equation (18),

$$I(\hat{\varepsilon}_d) \propto \mathrm{Tr}\{\sigma_e(t) D(\hat{\varepsilon}_d)\}$$

The excited state density matrix, σ_e, can be expressed in terms of the projection operators onto the excited state manifold (P_e) which operate on a transformed density matrix $\sigma(t)$:

B1) $$\sigma_e(t) = P_e \, \sigma(t) \, P_e$$

The purpose of this transformation is to eliminate the dependence of the density matrix on t before and after the exciting pulse by using the interaction representation. Thus, when one tries to solve the equations of motion in order to obtain the time evolution of the atomic system one no longer has to deal with the field-free Hamiltonian in the interaction representation.

One can use superscripts and subscripts to identify the transformed density matrix at various times or in various excited levels. For example,

$\sigma^+(+\infty)$ gives the density matrix after the exciting pulse has passed

$\sigma_i(t)$ gives the density matrix for the i^{th} level at time t

σ_o^+ identifies the ground state density matrix.

Let $\sigma_g = \sigma_{i-1}^+$ be the density matrix for the ground state and $\sigma_e = \sigma_i^+$ be the first excited state density matrix after one-photon excitation. Using the weak-pumping approximation, Silverman et al.[18] have shown that:

B2) $$\sigma_i^+ = k_o^{(i)}(+\infty) P_i \hat{\varepsilon}_i \cdot \vec{D} \; P_{i-1} \sigma_{i-1}^+ P_{i-1} \hat{\varepsilon}_i^* \cdot \vec{D} \; P_i$$

where P_i is the projection operator onto the i^{th} state.

This indicates that an excited state density matrix can be achieved from the ground state density matrix by projection of the latter onto the former via the electric dipole operator $\hat{\epsilon}\cdot\vec{D}$.

Another expression for σ_i^+ can be found by using the method of irreducible tensor operators as outlined by Happer.[22] Using the Wigner-Eckart theorem these operators can be expressed as:

B3) $$ {}^{F_i F_i' k_i}_{\quad T_{q_i}} = \sum_{m_i m_i'} \{(-1)^{F_i - m_i} (2k_i+1)^{1/2} |F_i m_i\rangle\langle F_i' m_i'| \begin{pmatrix} F_i & k_i & F_i' \\ m_i & q_i & m_i' \end{pmatrix} $$

where $\vec{F}_i$ and $\vec{F}_i'$ are the angular momenta $\vec{I}_i+\vec{J}_i$ and $\vec{I}_i'+\vec{J}_i'$ respectively for the two levels concerned

m_i and m_i' are the projections of $\vec{F}_i$ and $\vec{F}_i'$ onto the z-axis

The tensor operator T_k has rank k and 2k+1 components T_{kq} since $-k \le q \le k$.

Now σ_i^+ can be expressed as a linear sum of these irreducible tensor operators with coefficients α:

B4) $$ \sigma_i^+ = \sum (\alpha^{F_i F_i'}_{k_i q_i}) ({}^{F_i F_i' k_i}_{\quad T_{q_i}}) $$

B5) $$ \alpha^{F_i F_i'}_{k_i q_i} = \mathrm{Tr}\{\sigma_i^+ ({}^{F_i F_i' k_i}_{\quad T_{q_i}})^+\} $$

Now compose a recursion relation for the α's:

B6) $$ \alpha^{F_i F_i'}_{k_i q_i} = k_o^{(i)} (+\infty) \sum {}^{F_i F_i' F_{i-1} F_{i-1}'}_{k_i q_i A k_{i-1} q_{i-1}} (\alpha^{F_{i-1} F_{i-1}'}_{k_{i-1} q_{i-1}}) $$

The A coefficients project an α_{i-1} coefficient onto an α_i coefficient.

Using the recursion relations in (B2) and (B6) in the equation for α in (B5) one can finally arrive at an expression for the A coefficient:

B7) $$ {}^{F_i F_i' F_{i-1} F_{i-1}'}_{k_i q_i A k_{i-1} q_{i-1}} (\hat{\epsilon}_i) = \mathrm{Tr}\{P_i \hat{\epsilon}_i \cdot \vec{D} P_{i-1} ({}^{F_{i-1} F_{i-1}' k_{i-1}}_{\quad T_{q_{i-1}}})\} $$

$$\times \langle P'_{i-1} \hat{\epsilon}_i^* \cdot \vec{D} \, P'_i \rangle ({}^{F_i F'_i}_{k_i q_i} T)^+ \}$$

$$= \sum \langle F_i M_i | F_i M_i \rangle \langle F_i M_i | \hat{\epsilon}_i \cdot \vec{D} | F_{i-1} M_{i-1} \rangle$$

$$\times \langle F_{i-1} M_{i-1} | (-1)^{F_{i-1} - M_{i-1}} (2k_{i-1}+1)^{1/2} \begin{pmatrix} F_{i-1} & k_{i-1} & F'_{i-1} \\ -M_{i-1} & q_{i-1} & M'_{i-1} \end{pmatrix} | F_{i-1} M_{i-1} \rangle$$

$$\times \langle F'_{i-1} M'_{i-1} | F'_{i-1} M'_{i-1} \rangle \langle F'_{i-1} M'_{i-1} | \hat{\epsilon}_i^* \cdot \vec{D} | F'_i M'_i \rangle$$

$$\times \langle F'_i M'_i | (-1)^{F_i - M_i} (2k_i+1)^{1/2} \begin{pmatrix} F_i & k_i & F'_i \\ -M_i & q_i & M'_i \end{pmatrix} | F'_i M'_i \rangle \langle F_i M_i | F_i M_i \rangle$$

The summation is over $F_{i-1}, M_{i-1}, F'_{i-1}, M'_{i-1}, k_{i-1}, q_{i-1}, M_i$ and M'_i. This complicated expression can be simplified using the Wigner-Eckart theorem and graphical techniques as shown here:[20]

$$A^{F_i F'_i F_{i-1} F'_{i-1}}_{k_i q_i k_{i-1} q_{i-1}}(\hat{\epsilon}_i) = \sum \{ [\sum_{Q_i} (-1)^{Q_i} \epsilon_{-Q_i} (-1)^{F_i - M_i} \begin{pmatrix} F_i & 1 & F_{i-1} \\ -M_i & Q_i & M_{i-1} \end{pmatrix}$$

$$\times (2F_i+1)^{1/2} \langle F_i \| D_1 \| F_{i-1} \rangle]$$

$$\times [(-1)^{F_{i-1} - M_{i-1}} (2k_{i-1}+1)^{1/2} \begin{pmatrix} F_{i-1} & k_{i-1} & F'_{i-1} \\ -M_{i-1} & q_{i-1} & M'_{i-1} \end{pmatrix}$$

$$\times [\sum_{Q'_i} (-1)^{Q'_i + F'_{i-1} - M'_{i-1}} \epsilon_{-Q'_i} \begin{pmatrix} F'_{i-1} & 1 & F'_i \\ -M'_{i-1} & Q'_i & M'_i \end{pmatrix} (2F'_{i-1}+1)^{1/2} \langle F'_{i-1} \| D_1 \| F'_i \rangle]$$

$$\times [(-1)^{F_i - M_i} (2k_i+1)^{1/2} \begin{pmatrix} F_i & k_i & F'_i \\ -M_i & q_i & M'_i \end{pmatrix}]\}$$

$$= \sum_{\substack{F_{i-1} F'_{i-1} \\ k_{i-1} q_{i-1}}} (-1)^{-Q_i} [(2k_i+1)(2k_{i-1}+1)(2F_i+1)(2F'_{i-1}+1)]^{1/2}$$

$$\times \langle F_i \| D_1 \| F_{i-1} \rangle \langle F'_{i-1} \| D_1 \| F'_i \rangle$$

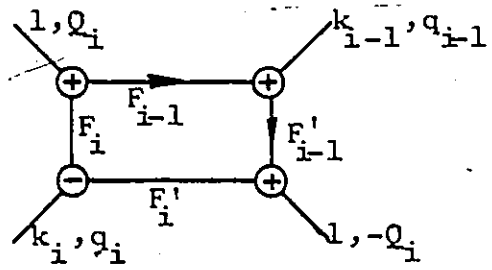

where Q_i indicates the polarization of the light.

Using the identity $\sum_x (2x+1)$ 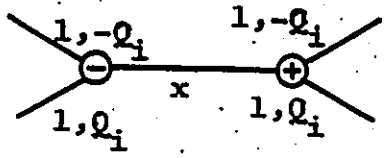 $= 1$

in a fusion with the above graphical symbol:

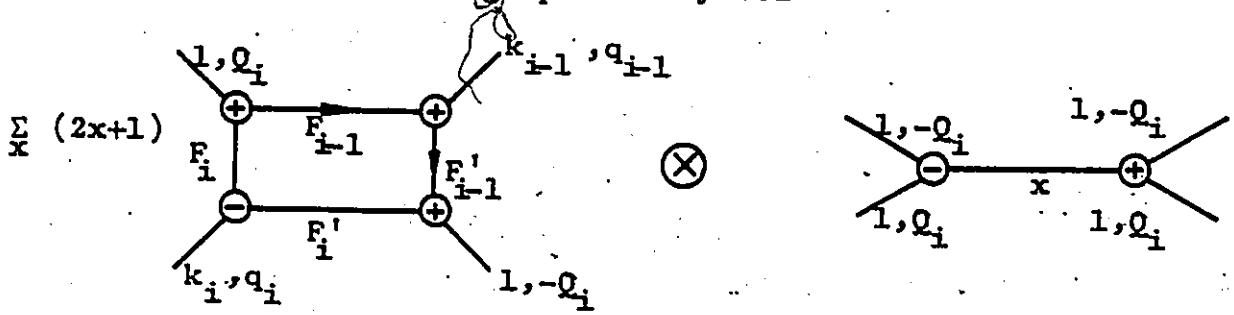

$= \sum_x (2x+1)$ 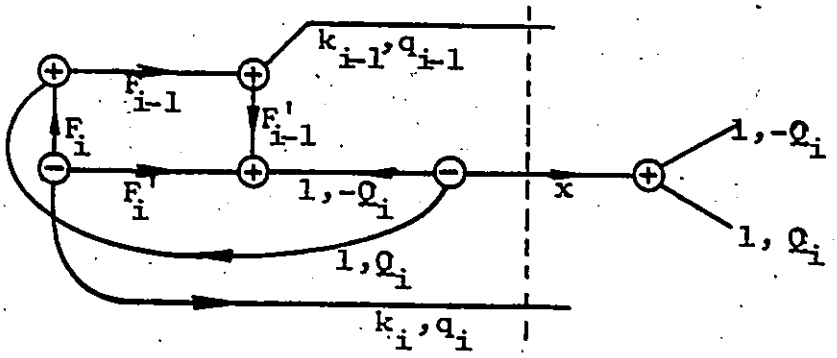

$= \sum_x (2x+1)$ 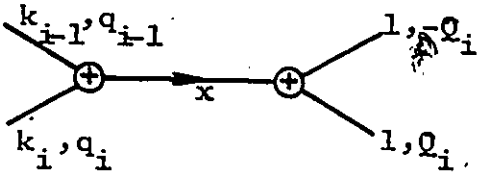

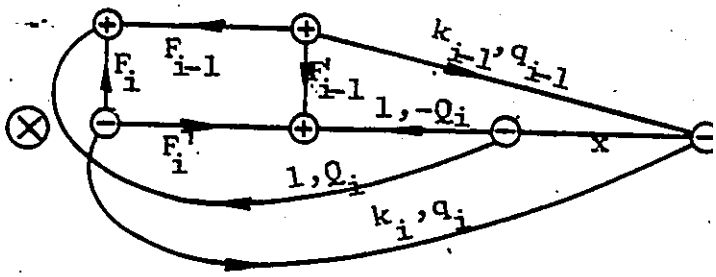

$$= \sum_x (-1)^{x+k_i+q_i} (2x+1) \begin{pmatrix} 1 & 1 & x \\ Q_i & -Q_i & 0 \end{pmatrix} \begin{pmatrix} x & k_{i-1} & k_i \\ 0 & q_{i-1} & q_i \end{pmatrix}$$

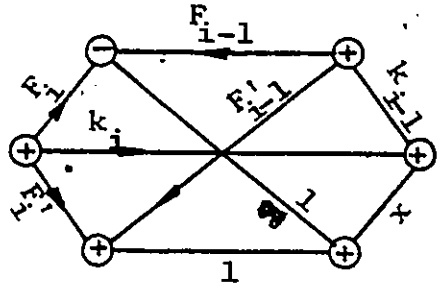

$$= \sum_x (2x+1)(-1)^{F_i+F_{i-1}+k_i+q_i+1} \begin{pmatrix} 1 & 1 & x \\ Q_i & -Q_i & 0 \end{pmatrix} \begin{pmatrix} x & k_{i-1} & k_i \\ 0 & q_{i-1} & q_i \end{pmatrix} \begin{Bmatrix} 1 & 1 & x \\ F_i & F'_i & k_i \\ F_{i-1} & F'_{i-1} & k_{i-1} \end{Bmatrix}$$

Also $\langle F_i \| D_1 \| F_{i-1} \rangle = (-1)^{F_{i-1}+J_i+I+1} (2F_{i-1}+1)^{1/2} (2J_i+1)^{1/2}$

$$x \begin{Bmatrix} F_i & F_{i-1} & 1 \\ J_{i-1} & J_i & I \end{Bmatrix} \langle J_i \| D_1 \| J_{i-1} \rangle$$

$$= (-1)^{F_{i-1}+J_{i-1}+J_i+L_i+S+I}[(2J_i+1)(2J_{i-1}+1)(2F_{i-1}+1)(2L_i+1)]^{1/2}$$

$$x\begin{Bmatrix} F_i & F_{i-1} & 1 \\ J_{i-1} & J_i & I \end{Bmatrix}\begin{Bmatrix} J_i & J_{i-1} & 1 \\ L_{i-1} & L_i & S \end{Bmatrix} \langle L_i \| D_1 \| L_{i-1} \rangle$$

Similarly $\langle F'_{i-1} \| D_1 \| F'_i \rangle = (-1)^{I+S+F_i+L'_{i-1}+J'_{i-1}+J'_i}[(2F_i+1)(2L'_{i-1}+1)(2J_i+1)]^{1/2}$

$$x\,(2J'_{i-1}+1)^{1/2}\langle L'_{i-1} \| D_1 \| L'_i \rangle\begin{Bmatrix} F'_{i-1} & F'_i & 1 \\ J'_i & J'_{i-1} & I \end{Bmatrix}\begin{Bmatrix} J'_{i-1} & J'_i & 1 \\ L'_i & L'_{i-1} & S \end{Bmatrix}$$

This gives finally:

$$\begin{aligned} {}^{F_iF'_i\ F_{i-1}F'_{i-1}}_{k_iq_i\ k_{i-1}q_{i-1}}A(Q_i) = \Sigma\{&(-1)^{2(I+S)+F_{i-1}+F_i+J_i+J'_i+J_{i-1}+L_i+L'_{i-1}+k_i+q_i+1-Q_i} \\ &x[(2k_i+1)(2k_{i-1}+1)(2F_i+1)(2F_{i-1}+1)(2J_i+1)(2J'_{i-1}+1)]^{1/2} \\ &x[(2F_i+1)(2F'_{i-1}+1)(2J'_i+1)(2J_{i-1}+1)(2L_i+1)(2L'_{i-1}+1)]^{1/2} \\ &x\begin{Bmatrix} F_i & F_{i-1} & 1 \\ J_{i-1} & J_i & I \end{Bmatrix}\begin{Bmatrix} F'_{i-1} & F'_i & 1 \\ J'_i & J'_{i-1} & I \end{Bmatrix}\begin{Bmatrix} J_i & J_{i-1} & 1 \\ L_{i-1} & L_i & S \end{Bmatrix}\begin{Bmatrix} J'_{i-1} & J_i & 1 \\ L'_i & L'_{i-1} & S \end{Bmatrix} \\ &x\ \sum_x (2x+1)\begin{pmatrix} 1 & 1 & x \\ Q_i & -Q_i & 0 \end{pmatrix}\begin{pmatrix} x & k_{i-1} & k_i \\ 0 & q_{i-1} & q_i \end{pmatrix}\begin{Bmatrix} 1 & 1 & x \\ F_i & F'_i & k_i \\ F_{i-1} & F'_{i-1} & k_{i-1} \end{Bmatrix} \end{aligned} \qquad \text{B8)}$$

The first summation is over all possible combinations of the ground state, the first and second excited states and the final state. The summation over x is only for x=0,1 and 2 since otherwise the 9-J symbol is zero.

Using rotational operators $R_{kq}(\varphi_i, \theta_i, 0)$, having as arguments the Euler angles, one can transform the A coefficients such that:

$$\begin{aligned} {}^{F_iF'_i\ F_{i-1}F'_{i-1}}_{k_iq_i\ k_{i-1}q_{i-1}}A(\hat{\varepsilon}_i) &= {}^{F_iF'_i\ F_{i-1}F'_{i-1}}_{k_iq_i\ k_{i-1}q_{i-1}}A(Q_i, \theta_i, \varphi_i) \\ &= \sum_q R^{(k_i)}_{q_iq}(\varphi_i, \theta_i, 0)\,{}^{F_iF'_i\ F_{i-1}F'_{i-1}}_{k_iq_i\ k_{i-1}q}A(Q_i) \\ &\quad x\,[R^{(k_{i-1})}(\varphi_i, \theta_i, 0)]^{(-1)}_{qq_{i-1}} \end{aligned} \qquad \text{B9)}$$

Thus, the angular portion of the A coefficients is contained only within the R operators.

APPENDIX C

Intensity Profile for $nD_{3/2}$ Levels of Potassium I

The following intensity profile, including hyperfine quantum beats, for the $nD_{3/2}$ levels of potassium was performed by the author using a PET Commodore microcomputer. The equation for the intensity I is given by:

$$I = I_o + \sum_f I_{mf}\cos(\omega_f t) \qquad (C1)$$

where I_o is the unmodulated signal, I_{mf} are the modulated signals and the summation is over all possible modulation frequencies f.

1) For $F_o=1$:

Unmodulated Signal

$$I_o = 6.16 + 14.62[\tfrac{1}{2}(3\cos^2\theta_d - 1)] + 5.93[\tfrac{1}{2}(3\cos^2\theta_1 - 1)] + 16.59[\sin^2\theta_d \sin^2\theta_1 \cos^2(\varphi_1 - \varphi_d)] - 3.50[\sin 2\theta_d \sin 2\theta_1 \times \cos(\varphi_1 - \varphi_d)] - 1.15[\tfrac{1}{2}(3\cos^2\theta_d - 1)\tfrac{1}{2}(3\cos^2\theta_1 - 1)]$$

Modulated Signal

$$I_m(\nu_{01}) = 0$$

$$I_m(\nu_{12}) = 0.78[\tfrac{1}{2}(3\cos^2\theta_d - 1)] + 5.78[\sin^2\theta_d \sin^2\theta_1 \cos 2(\varphi_1 - \varphi_d)] - 1.66[\sin 2\theta_d \sin 2\theta_1 \cos(\varphi_1 - \varphi_d)] + 0.388[\tfrac{1}{2}(3\cos^2\theta_d - 1)\tfrac{1}{2}(3\cos^2\theta_1 - 1)]$$

$$I_m(\nu_{13}) = 4.19[\tfrac{1}{2}(3\cos^2\theta_d - 1)] - 1.20[\sin^2\theta_d \sin^2\theta_1 \cos 2(\varphi_1 - \varphi_d)] - 1.38[\sin 2\theta_d \sin 2\theta_1 \cos(\varphi_1 - \varphi_d)] + 2.99[\tfrac{1}{2}(3\cos^2\theta_d - 1)\tfrac{1}{2}(3\cos^2\theta_1 - 1)]$$

$$I_m(\nu_{23}) = 15.30[\tfrac{1}{2}(3\cos^2\theta_d - 1)] - 4.92[\sin^2\theta_d \sin^2\theta_1 \cos 2(\varphi_1 - \varphi_d)] + 6.15[\sin 2\theta_d \sin 2\theta_1 \cos(\varphi_1 - \varphi_d)] - 8.74[\tfrac{1}{2}(3\cos^2\theta_d - 1)\tfrac{1}{2}(3\cos^2\theta_1 - 1)]$$

$$I_m(\nu_{02}) = -0.66[\tfrac{1}{2}(3\cos^2\theta_d - 1)] - 2.62\times 10^{-10}[\sin^2\theta_d \sin^2\theta_1 \times \cos 2(\varphi_1 - \varphi_d)] - 0.37[\sin 2\theta_d \sin 2\theta_1 \cos(\varphi_1 - \varphi_d)] + 0.66[\tfrac{1}{2}(3\cos^2\theta_d - 1)\tfrac{1}{2}(3\cos^2\theta_1 - 1)]$$

2) For $F_o=2$:

Unmodulated Signal

$$I_o = 3.70 + 3.82[\tfrac{1}{2}(3\cos^2\theta_d-1)] + 5.27[\tfrac{1}{2}(3\cos^2\theta_l-1)]$$
$$+9.82[\sin^2\theta_d\sin^2\theta_l\cos 2(\varphi_l-\varphi_d)]$$
$$-0.698[\sin 2\theta_d\sin 2\theta_l\cos(\varphi_l-\varphi_d)]$$
$$-3.13[\tfrac{1}{2}(3\cos^2\theta_d-1)\tfrac{1}{2}(3\cos^2\theta_l-1)]$$

Modulated Signal

$$I_m(\nu_{01}) = 0$$
$$I_m(\nu_{12}) = 17.23[\tfrac{1}{2}(3\cos^2\theta_d-1)]+2.99[\sin^2\theta_d\sin^2\theta_l\cos 2(\varphi_l-\varphi_d)]$$
$$-0.519[\sin 2\theta_d\sin 2\theta_l\cos(\varphi_l-\varphi_d)]$$
$$-0.406[\tfrac{1}{2}(3\cos^2\theta_d-1)\tfrac{1}{2}(3\cos^2\theta_l-1)]$$
$$I_m(\nu_{02}) = 9.58[\tfrac{1}{2}(3\cos^2\theta_d-1)]-0.76\times10^{-9}[\sin^2\theta_d\sin^2\theta_l$$
$$\times\cos 2(\varphi_l-\varphi_d)] - 1.08[\sin 2\theta_d\sin 2\theta_l\cos(\varphi_l-\varphi_d)]$$
$$+ 1.92[\tfrac{1}{2}(3\cos^2\theta_d-1)\tfrac{1}{2}(3\cos^2\theta_l-1)]$$
$$I_m(\nu_{23}) =-7.58[\tfrac{1}{2}(3\cos^2\theta_d-1)]-1.72[\sin^2\theta_d\sin^2\theta_l\cos 2(\varphi_l-\varphi_d)]$$
$$+3.23[\sin 2\theta_d\sin 2\theta_l\cos(\varphi_l-\varphi_d)]$$
$$-4.97[\tfrac{1}{2}(3\cos^2\theta_d-1)\tfrac{1}{2}(3\cos^2\theta_l-1)]$$
$$I_m(\nu_{13}) =-2.51[\tfrac{1}{2}(3\cos^2\theta_d-1)]-0.718[\sin^2\theta_d\sin^2\theta_l\cos 2(\varphi_l-\varphi_d)]$$
$$-0.831[\sin 2\theta_d\sin 2\theta_l\cos(\varphi_l-\varphi_d)]$$
$$+1.80[\tfrac{1}{2}(3\cos^2\theta_d-1)\tfrac{1}{2}(3\cos^2\theta_l-1)]$$

For definitions of the frequencies ν_{ij} see Figure 1.

BIBLIOGRAPHY

1. Bates, D.R. & Damgaard, A., Phil.Trans.R.Soc. 242, 101 (1949)
2. Warner,B., Mon.Not.R.Astron.Soc. 139, 1-34 & 115-128 (1968)
3. Edmonds, A.R., Picart, J., Tranminh, N. & Pullen, R., J.Phys.B 12, 2781 (1979)
4. Teppner, U. & Zimmermann, P., Astrn.& Astrophys. 64, 215 (1978)
5. Neil, W.S., M.Sc.Thesis, U.of Windsor (1982)
6. Copley, G. & Krause, L., Can.J.Phys. 47, 533 (1969)
7. Link, J.K., J.Opt.Soc.Am. 56, 1195 (1966)
8. Schmieder,R.W., Lurio,A. & Happer,W., Phys.Rev. 173,76 (1968)
9. Svanberg, S., Phys.Scripta 4, 275 (1971)
10. Bulos, B.R., Gupta. R. & Happer, W., J.Opt.Soc.Am. 66, 426 (1976)
11. Abramowitz, M. & Stegun, I.A. Handbook of Mathematical Functions National Bureau of Standards, Washington, D.C. (1965)
12. Gounand, F., J.Physique 40, 457 (1979)
13. Corliss, C. & Sugar, F., J.Phys.Chem.Ref.Data 8, 1109 (1979)
14. Wing, W.H. & Farley, J.W., Phys.Rev.A 23, 2397 (1981)
15. Lindgård, A. & Nielsen, S.E., At.Data Nucl.Data Tables 19, 533 (1977)
16. Bebb, A.B., Phys.Rev., 149, 25 (1966)
17. Haroche, S., Topics in Applied Physics 13 High Resolution Laser Spectroscopy, Ed. K.Shimoda Springer-Verlag (1976)
18. Silverman, M.P., Haroche, S. & Gross, M. Phys.Rev. A 18, 1507-1516 & 1517-1528 (1978)
19. Luypaert, R. & Van Craen, J., J.Phys.B 10, 3627 (1977)
20. Brink, D.M. & Satchler, G.R., Angular Momentum (Second Edition) Oxford Press (1971)
21. Burgess, A. & Seaton, M.J., Mon.Not.R.Astron.Soc. 120, 1 (1960)
22. Happer, W., Rev.Mod.Phys. 44, 174 (1972)
23. Pendrill, L.R., J.Phys.B 10, L469 (1977)

24. Harper, C.D., Wheatley, S.E. & Levenson, M.D., J.Opt.Soc.Am. 67, 579 (1977)

25. Gounand, F., Cuvellier, J., Fournier, P.R. & Berlande, J., J.Physique Lettres 37, L169 (1976)

26. Hugon, M., Gounand, F. & Fournier, P.R., J.Phys.B 13, L109 (1980)

27. Condon, E.U. & Shortley, G.H., The Theory of Atomic Spectra Cambridge University Press (1957)

28. Gallagher, T.F. & Cooke, W.E., Phys.Rev.Lett. 42, 835 (1976)

29. Gallagher, T.F. & Cooke, W.E., Phys.Rev.A 20, 670 (1979)

30. Pendrill, L.R. & Series, G.W., J.Phys.B 11, 4049 (1978)

31. Belin, G., Holmgren, L., Lindgren, I. & Svanberg, S., Phys.Scripta 12, 287 (1975)

32. Laser Dyes, Exciton Chemical Company Dayton, Ohio (1980)

33. Atomic Transitions By Element NBS Monograph 32 Part I, Washington, D.C. (1961)

34. Nesmeyanov, A.N., Vapour Pressure of the Elements Academic Press, New York (1963)

35. Coates, P.B., J.Phys.D 6, 1159 (1973)

36. Heavens, O.S., J.Opt.Soc.Am. 51, 1058 (1961)

37. Niefer, R.J., Ph.D.Thesis, U. of Windsor (1983)

38. Thomas, L.H., J.Chem.Phys. 22, 1758 (1954)

39. Seaton, M.J., Mon.Not.R.Astron.Soc. 118, 513 (1960)

40. Rogers, P.C., FRANTIC, Program for analysis of exponential growth and decay curves, M.I.T. Laboratory of Nuclear Sciences Technical Report No.76 (1962-unpublished)

VITA AUCTORIS

I was born on September 27,1957 in Toronto, Ontario where I attended Brebeuf College School, attaining an Ontario Scholarship after Grade 13. From there I entered the University of Toronto on an entrance scholarship and eventually received a Bachelor of Science degree in the physics program. I then moved to Windsor to work on a Master of Science degree in experimental physics at the University of Windsor with the aid of a postgraduate scholarship.